Geochimica et Cosmochimica Acta 391 (2025) 158–176

Contents lists available at ScienceDirect

Geochimica et Cosmochimica Acta

journal homepage: www.elsevier.com/locate/gca

Magnesium isotope composition of volcanic rocks from cold and warm subduction zones: Implications for the recycling of subducted serpentinites and carbonates

Wei Zhang [a,b], Hiroshi Kitagawa [a,*], Fang Huang [b]

[a] The Pheasant Memorial Laboratory for Geochemistry and Cosmochemistry, Institute for Planetary Materials, Okayama University, Misasa 6820193, Tottori, Japan
[b] CAS Key Laboratory of Crust-Mantle Materials and Environments, School of Earth and Space Sciences, University of Science and Technology of China, Hefei 230026, China

ARTICLE INFO

Associate editor: Shichun Huang

Keywords:
Magnesium isotopes
Arc magmas
Mantle wedge serpentinite
Slab serpentinite
Carbonate recycle

ABSTRACT

Magnesium (Mg) isotopes are regarded as a sensitive tracer to the contribution from subducted serpentinites and carbonates. However, the source, distribution, and controlling factors of the Mg isotope composition of arc magmas remain unclear. In this study, we investigated the intra-arc and inter-arc variations in Mg isotope compositions of volcanic rocks from two typical cold subduction zones [NE Japan (NEJ) and Izu arcs] and a typical hot subduction zone [SW Japan (SWJ) arc] to address the question. The volcanic rocks from the frontal-arc regions of NEJ and Izu have isotopically heavy Mg (δ^{26}Mg = –0.20 to –0.08 ‰) compared to the mantle-like δ^{26}Mg values of most of volcanic rocks from SWJ and the rear regions of NEJ and Izu arcs (–0.28 to –0.17 ‰). It is also worth noting that NEJ arc includes samples with δ^{26}Mg values (–0.61 to –0.39 ‰) significantly lower than the mantle, but similar to the $<$ 110 Ma intra-continental basalts from eastern China, which is the first observation in modern arc rocks. No obvious effects of post-eruptive alteration, fractional crystallization, partial melting, or the addition of silicate-rich sediment and oceanic crust components could be identified in the Mg isotope compositions of these volcanic rocks. By contrast, the correlations between the δ^{26}Mg values and the proxy for serpentinite component (i.e., ^{11}B/^{10}B and Nb/B ratios) indicate that the component exerts a strong control on the Mg-isotopic signature of these arc rocks. Considering metamorphic reactions in subduction lithologies under *P-T* conditions postulated for these arcs, the variations in δ^{26}Mg values of these arc magmas are unlikely to have been controlled by dehydration of serpentinites in subducted oceanic lithosphere (slab serpentinite). Instead, the high-δ^{26}Mg values of frontal-arc rocks are delivered by the fluids from serpentinite formed in the lowermost part of the sub-arc mantle (mantle wedge serpentinite) in channelized flow. Comparatively, such a high-δ^{26}Mg signature is invisible in volcanic rocks from rear-arc regions of NEJ and Izu, and the entire SWJ, suggesting that the major Mg carriers in subducted serpentinites (e.g., talc, chlorite, and serpentine) were broken down completely before subducted slabs reached the depth beneath these volcanoes. Moreover, the volcanic rocks with low δ^{26}Mg values from the rear arc of NEJ are characterized by high La/Yb and U/Nb ratios as well as low Ti/Eu, Ti/Ti*, and Hf/Hf* ratios, suggesting the involvements of carbonates in their magma sources. The quantitative modeling suggests that $<$ 20 % of sedimentary carbonate (dolomite) was recycled into their mantle source, revealing that Mg-rich carbonate could be incorporated into a deep mantle wedge at rear-arc depths of 150–400 km in subduction zones.

1. Introduction

Compared to mid-ocean ridge basalts (MORB), volcanic rocks in island and continental arcs are enriched in large ion lithophile elements (LILE; K, Rb, Sr, Cs, and Ba) and light rare earth elements (light REE or LREE; La, Ce, and Pr) and depleted in high field strength elements (HFSE; Ti, Zr, Nb, Hf, and Ta). The distinct features between MORB and arc volcanic rocks are commonly attributed to the addition of slab-derived components to sources of the latter (Pearce and Peate, 1995). Slab-derived components are considered to originate from three main

* Corresponding author.
E-mail address: kitaga-h@cc.okayama-u.ac.jp (H. Kitagawa).

https://doi.org/10.1016/j.gca.2024.12.024
Received 4 January 2024; Accepted 17 December 2024
Available online 22 December 2024

lithologies; sediment (including silicate-rich and carbonate-rich sediments), altered oceanic crust (AOC), and serpentinized lithospheric mantle (referred to as slab serpentinite) (Schmidt and Poli, 1998; Bebout, 2007). Fluids released from a subducted slab are able to hydrate the overlying mantle, resulting in the formation of serpentinites in the lowermost part of sub-arc mantle wedge (mantle wedge serpentinite) (Deschamps et al., 2013). Thus, two types of serpentinites might exist beneath arcs; slab serpentinite within the slab and mantle wedge serpentinite within the mantle wedge. Mantle wedge serpentinites tend to have lower abundances of REE, higher abundances of LILE, and lower $^{11}B/^{10}B$ ratios than slab serpentinite, as the former rocks have experienced multiple melting events and addition of slab-derived fluids (Deschamps et al., 2013; Martin et al., 2020). Serpentinites of either type have high abundances of water (up to 14 wt%; Deschamps et al., 2013; Cannaò and Malaspina, 2018) and thus are considered to be a primary source of water cycling between the Earth's surface and interior via the process of plate subduction (Konrad-Schmolke et al., 2016). On the other hand, carbonates within subducted sediments are vital for tracing the deep carbon cycle, which refers to carbon in-gassing to the mantle through subduction and outgassing through magmatic and volcanic processes (e.g., Li et al., 2017; Shen et al., 2018).

The Mg isotope composition is considered to be sensitive to the involvement of subducted serpentinites and some carbonates (e.g., dolomite and high-Mg calcite) within subducted sediments (Fig. 1a; Teng, 2017; Shen et al., 2018), which are enriched in Mg compared to other lithologies within a subducted slab (MgO content up to 20 to 40 wt %; Baker and Burns, 1985). The $\delta^{26}Mg$ values of carbonates and carbonate-rich sediments are generally very low (Fig. 1a; −5 to −0.2 ‰), owing to preferential uptake of light Mg isotopes during their precipitations from seawater (e.g., Higgins et al., 2018; Pearce et al., 2012). By contrast, the $\delta^{26}Mg$ values of subducted serpentinites are considered to be relatively high (Fig. 1a; −0.24 to +0.03 ‰) as observed in altered abyssal peridotites (Hu et al., 2017; Liu et al., 2017; Teng, 2017), which overlap with anhydrous mantle rocks (−0.25 ± 0.04 ‰; Teng et al., 2010a; hereafter this is referred to as "mantle-like $\delta^{26}Mg$") and show higher $\delta^{26}Mg$ values. Enrichment of heavy Mg isotopes in subducted serpentinites is considered to be due to alteration processes (i.e., formation of serpentine or talc; Beinlich et al., 2014; de Obeso et al., 2021) via seawater infiltration into their protoliths (Boschi et al., 2013; Evans et al., 2014; Prigent et al., 2020).

Arc volcanic rocks are generally considered to have been derived from the melting of sources affected by mass and chemical transfers from subducted lithologies including serpentinites and sediments (Pearce and Peate, 1995). In addition, a few peculiar types of rocks also occur in some arcs via direct melting of subducted lithologies (Defant and Drummond, 1990; Shimoda et al., 1998). Productions of such magmas, referred to as adakite and high-Mg andesite, leave residues containing Mg-bearing mafic minerals (e.g., garnet). Hence, a significant variation in $\delta^{26}Mg$ values of volcanic rocks is anticipated within an arc or among arcs. Although published Mg isotope data for arc rocks are yet limited, significant heterogeneity between different arcs was revealed. Slightly heavier $\delta^{26}Mg$ values are found in some of the Cascadia and Makran arc lavas but are attributed mainly to the assimilation of crustal materials (*meta*-igneous or *meta*-sedimentary rocks) during fractional crystallization of parental magmas (Fig. 1b; Brewer et al., 2018; Pang et al., 2020). High $\delta^{26}Mg$ values were also observed in basalts from Amami Sankaku Basin formed at the arc inception of Izu-Bonin-Mariana arc (Fig. 1b; Yuan et al., 2023). However, these basalts lack typical slab-derived inputs (e.g., enrichments of Rb/Y and Nb/Y), hence the heavy Mg isotope composition is suggested to be inherited from their source containing recycled talc-bearing serpentinite components in the mantle prior to subduction initiation. Arc rocks from the Kamchatka and Costa Rica volcanoes have mantle-like $\delta^{26}Mg$ values, while those from the Lesser Antilles Islands and the Philippines are characterized by distinctly high $\delta^{26}Mg$ values (Fig. 1b; Teng et al., 2016; Li et al., 2017). Such a high-$\delta^{26}Mg$ feature was interpreted as reflecting the input of fluids released

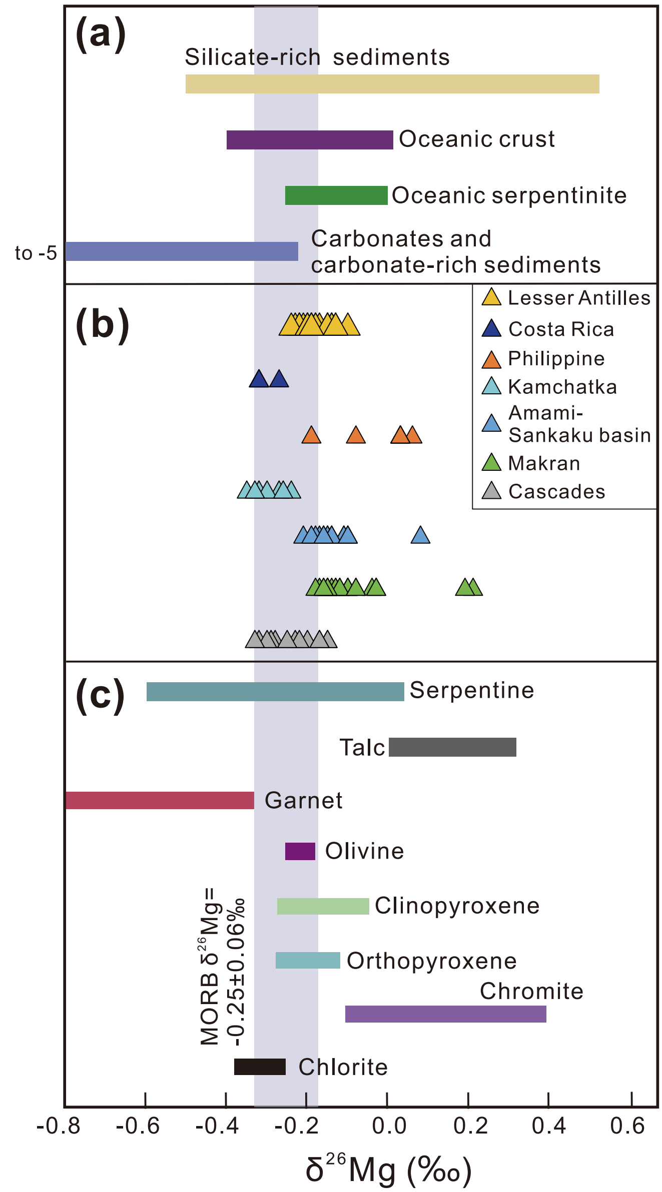

Fig. 1. The Mg isotopic compositions ($\delta^{26}Mg$ values) of (a) sediments (carbonate-rich and silicate-rich), oceanic crust (altered basalts) and serpentinites (altered ultramafic rocks) found on or within oceanic lithosphere (Teng et al., 2016; Hu et al., 2017; Li et al., 2017; Teng, 2017), (b) arc volcanic rocks [Kamchatka, Philippines, and Costa Rica: Li et al. (2017); Lesser Antilles: Teng et al. (2016); Makran: Pang et al. (2020); Cascades: Brewer et al. (2018); Amami-Sankaku Basin: Yuan et al. (2023)], and (c) major Mg-bearing minerals in sub-arc mantle (Teng, 2017; Stracke et al., 2018; Su et al., 2019; Meng et al., 2021). The light purple shaded area denotes the $\delta^{26}Mg$ value of unaltered MORB after Teng et al. (2010a).

from subducted serpentinites to magma sources (Teng et al., 2016; Li et al., 2017). The $\delta^{26}Mg$ values of volcanic rocks from these four arcs show positive correlations with the surface temperatures or depths of subducted slabs beneath the volcanoes of these arcs. Such correlations were attributed to the dehydration of serpentinite within the subducting oceanic lithosphere (Hu et al., 2020). As slab serpentinite resides in the slab interior with lower temperatures, it will retain fluids to deeper regions with higher temperatures (Syracuse et al., 2010). Therefore, slab serpentinites from a warm slab in a hot subduction zone or a slab in reararc depths (> 150 km) in a cold subduction zone (e.g., Lesser Antilles and Philippines) are considered to release fluids with heavy Mg isotopic composition (Walowski et al., 2015; Hu et al., 2020). Given that serpentinites in a subducting slab have significantly higher Mg and water contents than AOC (Deschamps et al., 2013; Scambelluri et al., 2019), the released fluids could have a significant impact on the Mg isotope signatures of the sub-arc mantle beneath these regions (Hu et al., 2020).

However, as mentioned above, serpentinites in a subduction zone have two origins; one is formed in an oceanic lithosphere prior to subduction (slab serpentinite), and the other is formed in the mantle wedge (mantle wedge serpentinite). The latter is formed at forearc depth by the shallow dehydration of slab and dragged down to the sub-arc region by subduction-induced mantle flow (Martin et al., 2020). Owing to the uptake of fluids enriched in heavy isotopes of Mg from the slab (as observed in altered abyssal peridotites), mantle wedge serpentinite might also be enriched in heavy Mg isotopes (Li et al., 2018). Such a high-δ^{26}Mg isotopic feature might be transferred to arc magmas via the dehydration of mantle wedge serpentinite upon increasing T through subduction into greater depths (> 90 km). Hence, a key question remains on the origin of heavy Mg isotope features in arc magmas (slab serpentinite versus mantle wedge serpentinite). Serpentinites in mantle wedge and subducting slab would have experienced different P-T paths; the former has a temperature ~200 to 400 °C higher than the latter (Syracuse et al., 2010; Lee and Kim, 2021). Accordingly, two serpentinites will release fluids at different depths and thermal conditions, affecting the Mg isotopic variation of arc rocks. However, few studies have conducted systematic investigations on the Mg isotope variation of arc volcanic rocks from different slab-depths (across-arc variation) within a subduction zone and among subduction zones with contrasting thermal conditions (hot versus cold subduction zones).

Furthermore, the incorporation of Mg-rich carbonates might also have remarkable effects on the Mg isotope compositions of subduction fluids and the mantle. As mentioned above, arc volcanic rocks were reported to have mantle-like or heavier Mg isotope features (Pogge von Strandmann et al., 2011; Teng et al., 2016; Li et al., 2017). The absence of carbonate signatures (light Mg isotope features) in arc magmas was interpreted to reflect the preferential dissolution of low-Mg carbonates (i.e., Ca-rich carbonates; calcite or aragonite) in slab-derived aqueous fluids at shallower depths (< 150 km; Pan et al., 2013), while such fluids predominantly inherit heavy Mg isotope features from altered abyssal peridotites (Teng et al., 2016; Wang et al., 2017). However, recent studies have documented the occurrence of intraplate basalts with light Mg isotope enrichment from eastern China where the Pacific plate subducts to and become stagnant at the mantle transition zone (Yang et al., 2012; Huang et al., 2015b; Wang et al., 2016; Tian et al., 2016; Li et al., 2017). These studies attributed the low-δ^{26}Mg features of these basalts to the melting of mantle metasomatized by subducted Mg-rich carbonates or carbonated eclogites in deep mantle (> 400 km). The evidence of carbonate contribution (low δ^{26}Mg values) at depths of 150 to 400 km was also reported in some continental collision zones (Shen et al., 2018; Tian et al., 2018). These observations raise a question regarding whether sedimentary Mg-rich carbonates could efficiently modify the Mg isotope composition of the mantle wedge at rear-arc depths of 150 to 400 km in oceanic subduction zones, which, if true, is important for tracing deep carbon.

In this study, we investigated the Mg isotope features of volcanic rocks from cold subduction zones with low slab-thermal gradient [Izu and Northeast Japan (NEJ) arcs] and a hot subduction zone [Southwest Japan arc (SWJ)] with high slab-thermal gradient, respectively (Fig. 2). New Mg isotope data are integrated with the existing elemental and isotopic data to (1) clarify the source of fluids with heavy Mg isotopic signatures and its transport mechanism to the source regions of arc

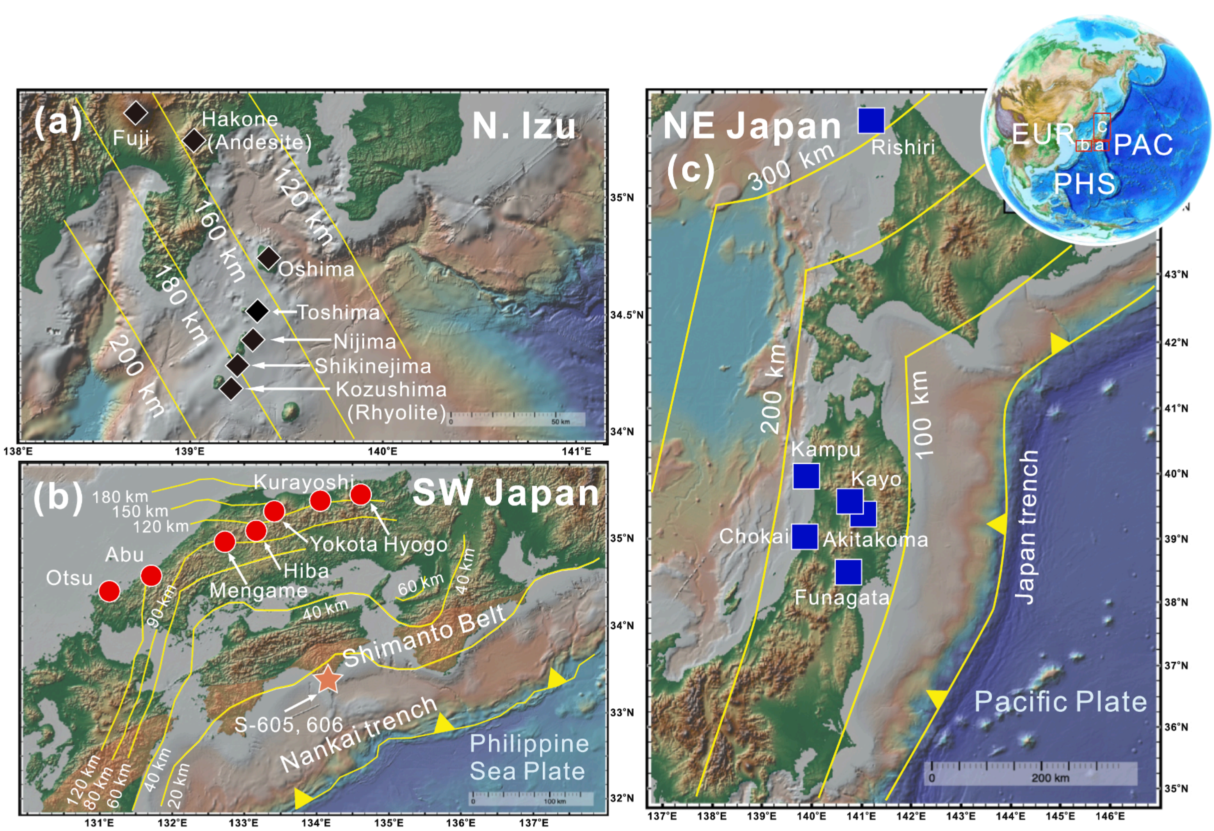

Fig. 2. Maps showing the locations of samples in (a) Izu arc, (b) SW Japan arc, and (c) NE Japan arc. The yellow lines represent the depth of the Wadati–Benioff zone or WBZ (Utsu, 1974; Ishida, 1992; Nakajima et al., 2009; Zhao et al., 2012). Black diamond, red circle, blue square, and orange star symbols represent the sampling sites in Izu (northern part), SW Japan (Chugoku district), NE Japan arcs, and the shales from the Shimanto Belt (shown as orange-colored regions), respectively. An inset map at the upper-right corner shows the plate configurations around these three arcs (PHS: Philippine Sea Plate; PAC: Pacific Plate; EUR: Eurasian Plate). The basemaps were created using GeoMapApp (https://www.geomapapp.org/).

magmas, (2) provide constraints on the impact of Mg-rich carbonates on arc magmas and carbon cycles at rear-arc depths from 150 and 400 km, and (3) reveal the Mg isotope systematics of subduction zones at different *P-T* conditions.

2. Geological setting

The volcanic rocks used in this study were selected from our collection of samples that are well characterized by the previous studies (e.g., Ishikawa and Nakamura, 1994; Moriguti and Nakamura, 1998; Moriguti et al., 2004; Pineda-Velasco et al., 2018; Nguyen et al., 2020; Zhang et al., 2023). These samples are mafic to intermediate volcanic rocks from three arcs (Fig. 2), namely, Izu, Northeast Japan (NEJ), and Southwest Japan (SWJ). The Izu arc is an intra-oceanic arc at the western margin of the Pacific (except for its northern extension where volcanic activity had occurred on a continental crust; Moriguti and Nakamura, 1998; Taylor and Nesbitt, 1998), whereas NEJ is a continental arc at the eastern margin of the Eurasia continent (Fig. 2a and c). Beneath the Izu and NEJ arcs, the Pacific plate is subducting via the Izu-Bonin and Japan trenches, respectively. Given that the subducting Pacific plate at the trenches is significantly old (129–135 Ma), those arcs represent two typical cold subduction zones (Syracuse et al., 2010). It is considered that slab-derived fluids in these arcs are dominated by aqueous solutions based on the geochemical features (e.g., elevated Ba/La and B/Nb) of volcanic rocks from frontal-arc regions (Ishikawa and Nakamura, 1994; Shibata and Nakamura, 1997; Taylor and Nesbitt, 1998).

Another marked feature of the Izu and NEJ arcs is that volcanoes distributed across these arcs show considerable ranges in depth to the slab (Wadati-Benioff zone or WBZ); 150 to 220 km for Izu and 130 to 300 km for NEJ, respectively (Fig. 2a and c; Utsu, 1974; Ishida, 1992; Nakajima et al., 2009). Clear across-arc variations in trace-element and isotopic composition are observed, which include the decreases in B/Nb ratio, δ^{11}B value [$\equiv \{(^{11}B/^{10}B)_{sample}/(^{11}B/^{10}B)_{standard} - 1\} \times 1000$], δ^{7}Li value [$\equiv \{(^{7}Li/^{6}Li)_{sample}/(^{7}Li/^{6}Li)_{standard} - 1\} \times 1000$], $^{87}Sr/^{86}Sr$ ratio, and $^{207}Pb/^{204}Pb$ ratio towards the rear-arc direction, and such features suggest a decrease in the amount of slab-derived fluids added to the source with increasing distance from the trench (e.g., Ishikawa and Nakamura, 1994; Moriguti and Nakamura, 1998).

In contrast, the SWJ arc is one of the hottest subduction zones in the world due to the subduction of an oceanic lithosphere [Philippine Sea (PHS) Plate] within a young oceanic basin (Shikoku Basin formed at 25–15 Ma; Kobayashi et al., 1995). The subducting PHS plate has a shallow dip angle (<30°) beneath the eastern part of SWJ (Chugoku district, Fig. 2b). Quaternary magmatism in this district occurred 90–120 km above the surface of the subducted PHS plate and is dominated by eruptions of high-Sr andesites and dacites (adakites), considered to have been derived by melting of the PHS plate (Fig. 2b; Feineman et al., 2013; Pineda-Velasco et al., 2018; Zhang et al., 2023). The loci of the adakite volcanoes spatially coincide with seismic discontinuities of the subducted PHS plate (Zhao et al., 2012). Thus, the magmatism is interpreted as the result of the slab melting at the plate tears (Pineda-Velasco et al., 2018). The Chugoku district also contains late Cenozoic volcanic rocks (12 Ma to Quaternary) with variable petrologic and geochemical features (Kimura et al., 2014; Nguyen et al., 2020). Among these rocks, mafic rocks with the geochemical characteristics of arc magmas (e.g., enrichments in Rb and Ba and depletions in Nb and Zr; Nguyen et al., 2020) are distributed in a narrow zone along the Sea of Japan. Hence, an across-arc geochemical variation in the Chugoku volcanic rocks is less clear (Fig. 2b). In the southern part of the Chugoku district, Cretaceous to Tertiary accretionary complexes, consisting of broken flysch units and tectonic mélange, are widely developed (Fig. 2b). The complexes are aligned subparallel to the Nankai trench, and termed the Shimanto Belt as a whole (Taira, 1988).

3. Samples and analytical methods

The samples used in this study ($n = 34$) are volcanic rocks from NEJ, Izu, and SWJ arcs. The major and trace element compositions of these samples and the Sr-Nd-Pb isotope compositions for selected samples were reported by previous studies (Kagami et al., 1989; Ishikawa and Nakamura, 1994; Shibata and Nakamura, 1997; Moriguti and Nakamura, 1998; Nakamura et al., 2002; Moriguti et al., 2004; Makishima and Nakamura, 2006; Lu et al., 2007; Feineman et al., 2013; Pineda-Velasco et al., 2018; Nguyen et al., 2020; Zhang et al., 2023; Supplementary Table S1). Petrographic characteristics of these samples are given in Supplementary Text S1.

The samples from the Izu arc ($n = 8$) are mafic to intermediate volcanic rocks with subordinate felsic rocks from the Izu Islands (Oshima, Toshima, Niijima, Shikinejima and Kozushima) and their northern extensional regions (Hakone and Fuji) on the Honshu Island (Fig. 2a; Ishikawa and Nakamura, 1994; Moriguti and Nakamura, 1998). All of them are Quaternary eruptive products (Ishizuka et al., 2006; Tani et al., 2011). Two samples are rhyolites (SHK-1 and KOZ-4), and others are basalts and basaltic andesites (Fig. 2a). All volcanic rocks are classified into sub-alkaline series. Earlier studies suggested that magmas in the arc are characterized by marked enrichments of LILE and depletions in HFSE (Kimura et al., 2010; Makishima and Nakamura, 2006; Lu et al., 2007; Taylor and Nesbitt, 1998).

The samples from the NEJ arc ($n = 13$) are basalts or basaltic andesites, collected from six Quaternary volcanoes (Fig. 2c; Shibata and Nakamura, 1997; Moriguti et al., 2004). These mafic rocks are classified into the sub-alkaline series and show a pronounced depletion in Nb and enrichments in LILE in normalized element abundance patterns (Shibata and Nakamura, 1997). The high LILE/HFSE ratios in these volcanic rocks are typical of arc magmas (e.g., Pearce and Peate, 1995).

The samples from the SWJ arc ($n = 13$) are basaltic rocks from 8 volcanic fields in the Chugoku district (southwestern end of Honshu Island) of the arc (Fig. 2b, 12 Ma to recent; Nguyen et al., 2020). These samples mainly consist of sub-alkaline mafic rocks with trace-element abundance patterns similar to arc basalts (e.g., marked depletion in Nb). All samples used in this study are with ages of 12.0 to 0.1 Ma. Two shale samples (S-605 and S-606) from the Shimanto Belt were also analyzed for their Mg isotope compositions, as these shales represent the type of oceanic sediments that might have been subducted to sub-arc depths and then incorporated into the magma source regions beneath the Chugoku district (Ishikawa and Nakamura, 1994). Selected major- and trace-element abundances and Pb, Li, and B isotope data are presented in Ishikawa and Nakamura (1994) and Moriguti and Nakamura (1998).

The Mg isotopic analyses were conducted at the Pheasant Memorial Laboratory for Geochemistry and Cosmochemistry, Institute for Planetary Materials, Okayama University at Misasa (Nakamura et al., 2002). Decomposition of samples follows Yokoyama et al. (1999). Powdered samples (~20 mg) were first dissolved using a concentrated HF-$HClO_4$ mixture for digestion, followed by evaporation with stepwise heating (120, 165, and 195 °C) to dryness. Dried samples were then dissolved using a concentrated $HClO_4$ for the digestion of fluoride precipitates with stepwise heating in the same manner as the first step (i.e., HF-$HClO_4$ digestion). Subsequently, the dried samples were dissolved using a 6 mol L^{-1} HCl, followed by evaporation at 110 °C until dryness. Decomposed samples were finally dissolved using 0.7 mol L^{-1} HCl for column chemistry. Magnesium was extracted and purified using a cation-exchange resin (AGMP-50) with 1.5 mol L^{-1} HCl (> 99% Mg yield). During column chemistry, rock standards (BHVO-2, AGV-1, and G-2) were processed simultaneously with unknown samples. Three rock standards yield average δ^{26}Mg values of −0.20 ± 0.04 ‰ (BHVO-2, n = 6), −0.13 ± 0.06 ‰ (AGV-1, n = 2), and −0.14 ± 0.02 ‰ (G-2, n = 2). Further details are found in Zhang et al. (2022). Isotopic measurements were performed by inductively coupled plasma mass spectrometry (ICP-MS) using a Thermo Fisher Neptune plus in static multicollection mode.

Instrumental mass bias and drift were corrected by bracketed analyses of an international standard [DSM3; Galy et al. (2003)]. The Mg isotope composition of a given sample is reported as $\delta^{n}Mg$ (‰) = $[(^{n}Mg/^{24}Mg)_{sample}/(^{n}Mg/^{24}Mg)_{DSM3} - 1] \times 1000$, where n refers to the mass 25 or 26. The long-term external precision (2SD, $N = 45$) is ± 0.06 ‰ for $\delta^{26}Mg$, which is assessed by replicate analyses of our in-house reference standard (PML-Mg1; Zhang et al., 2022) bracketed by DSM3. Major-element compositions of the Izu samples ($n = 5$), except for GSJ standard rocks, were analyzed by an X-ray fluorescence spectrometer. The analytical method of major elements is summarized in Supplementary Text S2.

4. Results

Magnesium-isotope data for the studied samples are provided in Table 1 and Table S1 in the Supplementary Material. The $\delta^{26}Mg$ values of the Izu and NEJ volcanic rocks show large or different variations compared with average MORB [−0.31 to −0.19 ‰; Teng et al., 2010a]; Izu arc rocks range from −0.20 ‰ to −0.10 ‰, and NEJ arc rocks range from −0.61 ‰ to −0.07 ‰ (Fig. 3a and b). The SWJ rocks have $\delta^{26}Mg$ values ranging from −0.28 ‰ to −0.17 ‰, which compare closely with the range of average MORB (Fig. 3c).

The $\delta^{26}Mg$ values of NEJ- and Izu-arc rocks show clear across-arc variations. Higher $\delta^{26}Mg$ values are found in frontal-arc regions, and lower $\delta^{26}Mg$ values are found in rear-arc regions (Fig. 3a and b). Izu rocks show a gradual decrease in $\delta^{26}Mg$ values with increasing WBZ depths (Fig. 3a), whereas NEJ rocks show an abrupt change in $\delta^{26}Mg$ values at front-to-rear-arc transition zones (WBZ = 150–170 km; Fig. 3b). In NEJ arc, the rear-arc rocks (except for Kampu volcanic rocks) have $\delta^{26}Mg$ values within the range of upper mantle, i.e., the occurrences of high $\delta^{26}Mg$ rocks are confined to frontal-arc regions in both arcs (Fig. 3b). It is worth noting that significantly low $\delta^{26}Mg$ values are found in Kampu volcanic rocks in the rear arc of NEJ, which range from –0.61 to –0.39 ‰ (Fig. 3b). It is also noted that $\delta^{11}B$ values in NEJ- and Izu-arc rocks also show clear and similar decreases from those in frontal-arc regions to those in rear-arc regions (Fig. 3a and b).

The WBZ-depth contours beneath SWJ are not parallel to the trench (Fig. 2b), indicating that the subduction angle varies laterally. It is shallower in the central part of the Chugoku district and is steeper in the eastern and western parts of the district (Zhao et al., 2012). Furthermore, the slab might have gaps in the rear-arc regions, interpreted as tears on the slab (Pineda-Velasco et al., 2018). Nguyen et al. (2020) suggested that the subduction angle and morphology of the slab have varied over the last 12 Myrs including the initiation of slab tearing at 5 Ma. Thus, the WBZ depths of each volcano at the time of eruptions could hardly be constrained. Instead, we use the perpendicular distance of a volcano to the Nankai trench as a proxy for an across-arc change in slab depth. To cancel or minimize a temporal change in the effect of slab distortion, we also compared $\delta^{26}Mg$ values and arc-trench distance separately for rocks erupted at 12–8 and 8–0 Ma. The volcanic activity in the latter period was confined to the regions above slab tears. In either period (12–8 Ma or 8–0 Ma), $\delta^{26}Mg$ values of SWJ rocks show insignificant correlations with the arc-trench distance (Fig. 3c).

Table 1
Mg isotopic composition of volcanic rocks from Northeast Japan arc, Izu arc, and Southwest Japan arc (Chugoku district).

Region	Sampling location	Sample name	W.B.Z. (km)	Arc-trench distance (km)	MgO (wt%)	$\delta^{25}Mg$ (‰)	2SD (‰)	$\delta^{26}Mg$ (‰)	2SD (‰)
NE Japan	Funagata	FUN07-01	135		5.76	−0.07	0.01	−0.17	0.01
	Funagata	Funagata68	135		8.4	−0.09	0.01	−0.18	0.02
	Funagata	Funagata72	135		5.02	−0.05	0.00	−0.11	0.02
	Akitakoma	820830–1	144		6.12	−0.08	0.01	−0.18	0.01
	Kayo	82928–3	145		2.95	−0.08	0.01	−0.16	0.01
	Kayo	82929–2	145		3.31	−0.03	0.02	−0.07	0.01
	Chokai	8930804–1	174		5.65	−0.12	0.01	−0.24	0.02
	Chokai	83606–2	174		5.24	−0.12	0.03	−0.25	0.05
	Kampu	K3-1	180		3.79	−0.19	0.01	−0.39	0.01
	Kampu	K3-2	180		3.69	−0.30	0.02	−0.59	0.03
	Kampu	K3-3	180		3.71	−0.31	0.02	−0.61	0.04
	Rishiri	R-1	300		5.51	−0.11	0.01	−0.22	0.03
	Rishiri	R-10	300		6.2	−0.14	0.00	−0.29	0.00
Izu	Oshima	OSF-1	150		5.00	−0.05	0.01	−0.11	0.02
	Oshima	JB-2	155		4.62	−0.06	0.04	−0.10	0.04
	Hakone	JA-1	160		1.57	−0.03	0.00	−0.12	0.06
	Fuji	JB-3	175		5.19	−0.07	0.01	−0.15	0.02
	Toshima	TO-2	180		6.61	−0.08	0.01	−0.19	0.02
	Nijima	NIW-1	185		5.08	−0.06	0.02	−0.15	0.03
	Shikinejima	SHK-1	200		0.07	−0.10	0.02	−0.20	0.05
	Kozushima	KOZ-4	210		0.28	−0.11	0.01	−0.20	0.03
SW Japan (Chugoku district)	Otsu	OTS-05		380	6.91	−0.11	0.04	−0.24	0.02
	Otsu	OTS-06		380	7.84	−0.10	0.01	−0.22	0.03
	Hiba	HIB-04		340	6.56	−0.11	0.01	−0.23	0.07
	Hiba	HIB-07		340	8.31	−0.12	0.01	−0.23	0.05
	Matsue	MAT-04		370	7.27	−0.07	0.05	−0.20	0.07
	Kurayoshi	MKM-01		340	5.07	−0.08	0.03	−0.17	0.04
	Kurayoshi	KUR-16		340	8.23	−0.10	0.05	−0.20	0.07
	Kurayoshi	KRW-02		340	8.35	−0.12	0.01	−0.25	0.02
	Mengame	MEN-02		345	9.71	−0.10	0.01	−0.17	0.01
	Abu	ABU-11		365	7.51	−0.09	0.03	−0.19	0.03
	Abu	ABU-21		365	8.30	−0.09	0.04	−0.18	0.03
	Abu	ABU-23		365	7.91	−0.10	0.01	−0.20	0.05
	Yokota	YOK-05		340	9.47	−0.13	0.02	−0.28	0.02
	N. Hyogo	INA-01		340	5.17	−0.09	0.00	−0.19	0.03
	N. Hyogo	HYO-15		340	7.46	−0.08	0.01	−0.19	0.01
Shimanto shale	Shikoku	605			9.47	−0.01	0.01	−0.08	0.03
	Shikoku	606			6.05	−0.06	0.00	−0.17	0.04

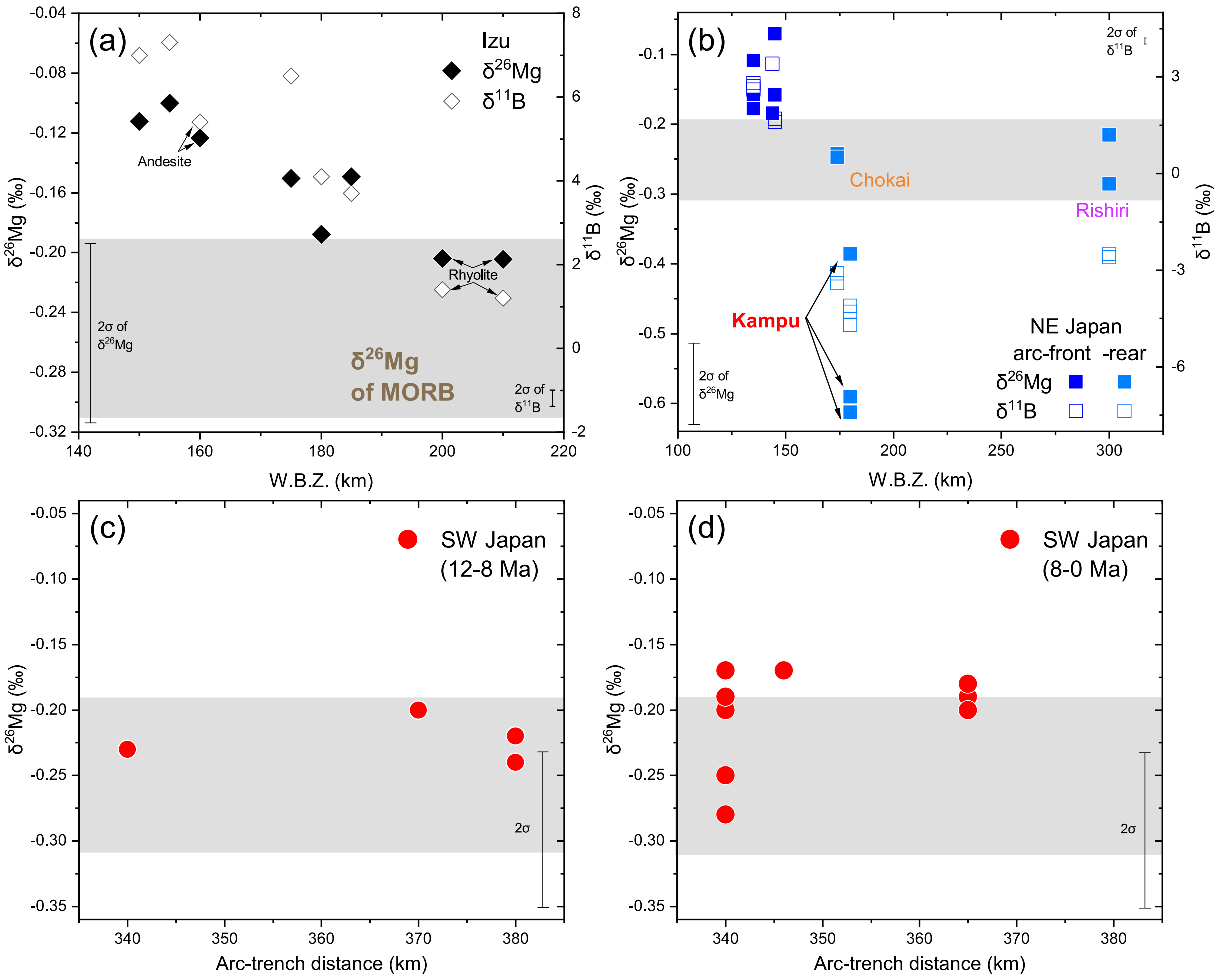

Fig. 3. Across-arc variation of the $\delta^{26}Mg$ values in the Izu, NEJ, and SWJ arcs. (a and b) the $\delta^{26}Mg$ values of Izu- and NEJ-arc volcanic rocks, respectively, plotted against the sub-volcanic WBZ depths. For comparison, the $\delta^{11}B$ values of the same volcanic rock samples, analyzed by Ishikawa and Nakamura (1994) and Moriguti et al. (2004), are shown. (c and d) the $\delta^{26}Mg$ values of SWJ-arc (Chugoku) volcanic rocks with ages of 12–8 Ma and 8–0 Ma plotted against perpendicular distances from the Nankai trench to each volcano. The range of $\delta^{26}Mg$ of unaltered MORB (–0.25 ± 0.06 ‰, shown by gray bands) is from Teng et al. (2010a). Uncertainty of $\delta^{26}Mg$ values for the studied samples is ± 0.06 ‰ (2σ external reproducibility).

5. Discussion

The key finding from Mg isotope investigations in this study is that NEJ- and Izu-arc rocks show clear across-arc variations in $\delta^{26}Mg$ values. Higher-than-MORB values (> –0.19 ‰) were found in frontal-arc rocks, while the values within the MORB range (–0.31 to –0.19 ‰) or lower than the MORB range (–0.61 to –0.39 ‰) were found in rear-arc rocks (Fig. 3a and b). In contrast, SWJ rocks do not show a clear across-arc change in their $\delta^{26}Mg$ values, which falls within the range of MORB (Fig. 3c and d). In the following sections, we evaluate the potential effects of post-eruptive alteration and pre-eruptive magmatic processes on the Mg isotope compositions of the studied samples and then explore the causes of Mg isotope variation within an arc and among arcs in relation to the *P-T* conditions of subduction zones.

5.1. Post-eruptive alteration

The variation in the $\delta^{26}Mg$ value of volcanic rocks could be related to post-eruptive processes, such as weathering and alteration via interaction with fluids (e.g., Tipper et al., 2010; Liu et al., 2014). Light Mg isotopes were preferentially dissolved into fluids and leached out from a rock. Consequently, the residual solid (weathered rock) becomes enriched in heavier isotopes than the original solid (unweathered rock). Main reservoirs of Mg in such weathered rocks are considered to be clay minerals formed by alteration of primary mafic silicates such as olivine and pyroxene (Teng et al., 2010b; Huang et al., 2012).

Most samples used in this study are fresh or least altered without the occurrence of secondary minerals such as zeolites, carbonates, and clay minerals (Supplementary Text S1). The loss on ignition (LOI) values of these samples fall within the range of –1 to 1.5 wt%, except for two samples (LOI > 1.5 wt%) from the Chugoku district in the SWJ arc (Fig. 4a, Table S1). The abundances of H_2O (as structural water, denoted as H_2O^+) are calculated to be < 1.5 wt% for most samples based on LOI, Fe abundances (expressed as Fe_2O_3 total), and $Fe^{2+}/\Sigma Fe$ ratios assumed for each sample (0.85 for basalts, 0.80 for andesites, and 0.75 for rhyolites, respectively). Relatively low H_2O abundances in the studied volcanic rocks also support little or insignificant addition of water (that facilitates the formation of secondary minerals) after their emplacements.

Most of the studied samples have the chemical index of alteration (CIA; Nesbitt and Young, 1982) ranging from 40 to 45 for mafic rocks and 47 to 51 for intermediate and felsic rocks, respectively. These values are well within the range of fresh rocks with mafic (30–50) and intermediate-felsic (45–55) compositions, respectively (Fig. 4b; Nesbitt and Young, 1982; Babechuk et al., 2014). A more detailed discussion is included in Supplementary Text S1.

In Fig. 4, $\delta^{26}Mg$ values are plotted against LOI and CIA values, showing no or insignificant correlations among these values for the

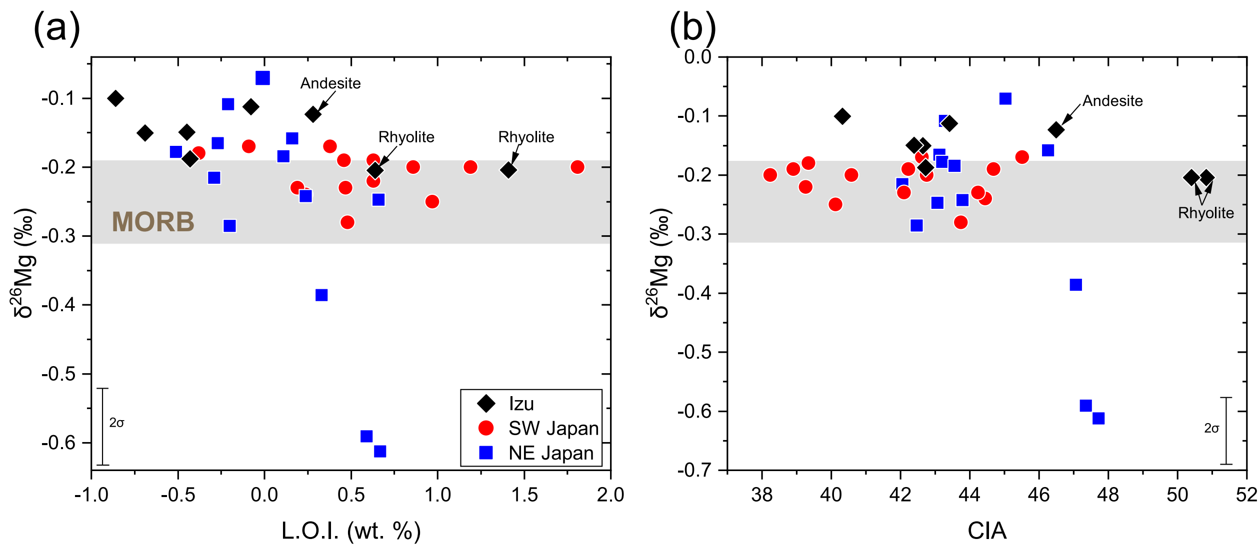

Fig. 4. The effect of alteration. (a) δ^{26}Mg values versus loss on ignition (LOI). (b) δ^{26}Mg values versus chemical index of alteration (CIA) defined as $[Al_2O_3/(Al_2O_3 + CaO^* + Na_2O + K_2O)] \times 100$ where oxide abundances are given in molecular proportions and CaO* denotes CaO abundances in the silicate fraction of a rock (Nesbitt and Young, 1982). The gray bars in both panels are the δ^{26}Mg values of unaltered MORB (Teng et al., 2010a). Uncertainty of δ^{26}Mg values for the studied samples is ± 0.06 ‰ (2σ external reproducibility).

studied rocks from the three arcs investigated here. Together, we consider that the post-eruptive alteration had a limited effect on the Mg isotope compositions of the studied rocks.

5.2. *Pre-emplacement processes*

5.2.1. *Fractional crystallization*

It was generally considered that fractional crystallization, involving these Mg-rich minerals, has little effect on Mg isotope compositions of differentiated magmas (Teng et al., 2007; Liu et al., 2011; Duan et al., 2023), whereas recent studies proposed that the cocrystallization of olivine and clinopyroxene could elevate δ^{26}Mg values by 0.04–0.05 ‰ compared to parental magma (Wang et al., 2021; Liu et al., 2022). The highest δ^{26}Mg value within our sample (a sample from NEJ, –0.07 ‰) is greater than the mean value of mantle (–0.25 ‰) by +0.18 ‰. The difference significantly exceeds the range of possible increases of δ^{26}Mg (0.04–0.05 ‰) caused by the crystallization of olivine and clinopyroxene. Moreover, remarked across-arc decrease of δ^{26}Mg values in volcanic rocks from Izu and NEJ arcs could be hardly explained by fractional crystallization (Fig. 3a and b). If Mg-isotope variation is dominated by fractional crystallization, it is anticipated that these volcanic rocks also show the correlation between MgO content and δ^{26}Mg values and across-arc variation in differentiation indices; Mg# value [$\equiv 100 \times Mg/(Mg + Fe^{2+})$] should increase in rocks from frontal-arc to rear-arc regions. Such features are not found in volcanic rocks in the studied arcs (Fig. 5a and Supplementary Fig. S4). Therefore, fractional crystallization of olivine and clinopyroxene did not play a major role in the production of δ^{26}Mg variations in these arcs.

We also examine the effect of volumetrically minor phases on Mg-isotope variations in the studied samples. Cr-spinel preferentially uptakes heavy Mg isotopes (Fig. 1c), and thus fractional crystallization of this mineral results in light Mg isotopic compositions in evolved magmas (Young et al., 2009; Su et al., 2017; Su et al., 2019). Fe-Ti oxides (titanomagnetite) are also suggested to lower δ^{26}Mg values of low-MgO differentiated magmas (Wang et al., 2021). However, the lack of correlations between the δ^{26}Mg values and Cr or TiO_2 contents in the studied samples (Fig. 5b and c) suggests that the scenarios for Cr-spinel or titanomagnetite involvement in the production of Mg isotope variations in these arcs are unlikely.

Accumulation of isotopically light ilmenite in the mantle source via crystallization of magma ocean was suggested to produce low δ^{26}Mg values in some lunar high-Ti basalts (Sedaghatpour et al., 2013). If this process occurred in parental magmas of our studied samples, the TiO_2 content should negatively correlate with δ^{26}Mg values (Huang et al., 2015b; Tian et al., 2016). However, the insignificant correlation rules this process out (Fig. 5c), consistent with the petrographic features of our samples (none of them show ilmenite accumulation; Supplementary Text S1). We thus consider that fractional crystallization did not play a major role in producing the variation in δ^{26}Mg values in volcanic rocks from the studied arcs.

5.2.2. *Partial melting*

Major mantle minerals (olivine and pyroxene) were generally considered to induce undetectable change in Mg isotope composition of mantle-derived magmas via partial melting of their-bearing lithologies (Teng et al., 2007, 2010a; Stracke et al., 2018; Liu et al., 2023; Detailed discussion is included in Supplementary Text S3).

Garnet preferentially incorporates lighter Mg isotopes, thus a melt in equilibrium with a residual source containing substantial garnets could have high-δ^{26}Mg values (Wang et al., 2015; Zhong et al., 2017; Stracke et al., 2018; Fig. 1c). A magma derived from a garnet-bearing source is anticipated to show high LREE/HREE (e.g., La/Yb) or middle rare earth element (MREE, e.g., Sm, Dy)/HREE ratios (e.g., Dy/Yb). There are no significant correlations between the Dy/Yb ratio and δ^{26}Mg value among the studied volcanic rocks from any of these three arcs (Fig. 5d). We conclude that partial melting did not play a role in producing the observed Mg-isotopic variations.

5.2.3. *Crustal contamination*

Mg isotopic compositions of the upper and middle-lower continental crust are highly heterogeneous, with δ^{26}Mg ranging from −1.64 to +0.92 ‰ and from −0.72 to +0.19 ‰, respectively (Teng, 2017 and references therein). Therefore, the δ^{26}Mg value of an arc magma could also be altered via the assimilation of crustal materials with distinct δ^{26}Mg values (Brewer et al., 2018; Pang et al., 2020). Low-Mg and high-Si upper crustal rocks generally have lower solidus temperatures [mostly < 1000 °C; Johannes (1984)] than the temperatures of mantle-derived mafic magmas when they entered into the crust (> 1000 °C). It is therefore likely that the parental magmas of arc-volcanic rocks would react with upper crustal materials to some extent.

The main part of Izu arc is formed on a thin mafic upper crust (~10 km) underlain by felsic (tonalitic) middle crust (Suyehiro et al., 1996).

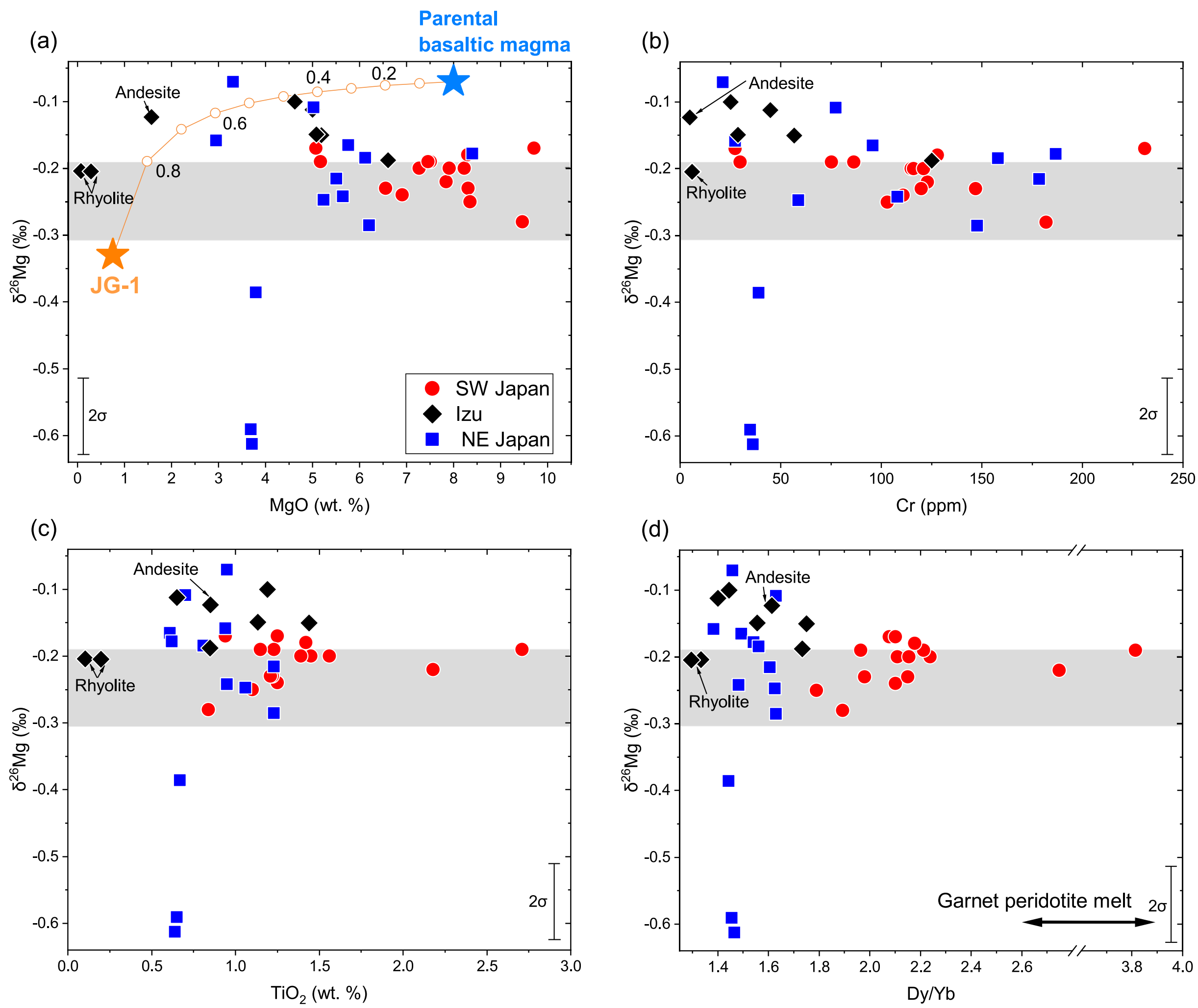

Fig. 5. δ^{26}Mg values plotted against the indices for the extent of fractional crystallization of a parental magma [(a) MgO, (b) Cr, and (c) TiO_2] or that of partial melting of a magma[(d) Dy/Yb]. In Fig. 5d, the range of Dy/Yb ratio of a melt derived from a garnet-facies peridotite, calculated for degrees of melting of 1–10 %, is shown by two head arrows. For calculation, the composition and mineralogy of a magma source are assumed to be the same as those of the primitive upper mantle (PUM; McDonough and Sun, 1995; McDonough and Rudnick, 1998), and the melting stoichiometry follows Fram et al. (1998). Partition coefficients between melt and residual mineral phases are from Kelemen et al. (2003). These parameters and results of the modeling are shown in Table S2. Uncertainty of δ^{26}Mg values for the studied samples is ± 0.06 ‰ (2σ external reproducibility). The gray bars in the panels show the range of δ^{26}Mg values of unaltered MORB (Teng et al., 2010a).

In contrast, volcanic fields in NEJ and SWJ arcs and the northmost end of Izu arc [Hakone (JA-1) and Fuji (JB-3)], located in Honshu Island, overlie thick (c. 30 km) upper crust consisting mainly of felsic rocks (Togashi et al., 2000; Zellmer, 2008; Wada and Wang, 2009). Therefore, we will focus on the potential effect of crustal contamination on the δ^{26}Mg values of volcanic rocks from these fields. A reference silicate rock, JG-1, provided by the GSJ, is a Cretaceous (92 Ma) granodiorite from Northeast Japan (Ando et al., 1989; Sudo et al., 1998), and might represent a possible crustal rock beneath NEJ volcanoes (Hunter and Blake, 1995). The [MgO] of 0.73–0.79 wt% and the δ^{26}Mg values from −0.31 to −0.35 ‰ are reported for JG-1 (Teng et al., 2015; Araoka and Yoshimura, 2019; Fig. 5a). This crustal rock is also characterized by high ^{86}Sr/^{87}Sr (0.711) and ^{207}Pb/^{204}Pb (15.627) ratios (Miyazaki and Shuto, 1998; Tanimizu and Ishikawa, 2006). The δ^{26}Mg values of the NEJ samples are positively correlated with ^{86}Sr/^{87}Sr (Fig. 7a; r^2 = 0.45) and ^{207}Pb/^{204}Pb (not shown; r^2 = 0.43). Extrapolation of these correlations to ^{86}Sr/^{87}Sr or ^{207}Pb/^{204}Pb ratio of the crustal assimilant yields its δ^{26}Mg value of > +0.1 ‰, which is distinctly different from the observed δ^{26}Mg (−0.31 to −0.35 ‰). Rather, the similarity between the δ^{26}Mg values of crustal rocks and mantle rocks suggests that the effect of crustal contamination might not be noticeable (Fig. 7a). A simple mass balance model is employed; [MgO] and the δ^{26}Mg value of upper crustal rocks are assumed to be 0.76 wt% and −0.33 ‰, respectively. The [MgO] of a parental magma, prior to crustal contamination, is assumed to be 8 wt% based on [MgO] of the least differentiated volcanic rocks in NEJ (Fujinawa, 1988). The δ^{26}Mg value of the parental magma is assumed to be –0.07 ‰ (the highest δ^{26}Mg among NEJ rocks and all samples). The modeling results (Fig. 5a) show that even 50 % of assimilation of crustal materials into a parental magma cannot shift the δ^{26}Mg to the lower values (–0.22 to –0.29 ‰) observed in the rear-arc volcanic rocks in NEJ. Accordingly, the assimilation of crustal rocks into mafic magmas could not solely explain the across-arc variation of δ^{26}Mg values in NEJ.

The crustal rocks in the SWJ are dominated by Paleogene granitic rocks (Jahn, 2010). In the northern part of Izu arc, volcanoes occur on the thick crust (~20–30 km; Aoki et al., 2019) containing felsic plutonic rocks (Kitamura et al., 2003). The δ^{26}Mg data for granitoids in these regions have not been published. However, due to the relatively low MgO contents of these granites (< 4 wt%; Kutsukake, 2002; Li and Ishihara, 2013), high volumes of assimilated granites would be required in mass balance to affect the Mg isotope composition of parental magmas of these arc rocks, which is unlikely. A detailed discussion about the effect based on previous studies is summarized in Supplementary Text S4.

5.3. Subduction inputs

As discussed above, neither post-eruptive alteration, fractional crystallization nor crustal contamination explain the Mg isotope features in volcanic arc rocks from our studied arcs. Alternatively, this variation could be caused by inputs from the subducted slab into the magma sources. Magnesium is soluble to variable extents in fluids released from variable lithologies within a subducted oceanic lithosphere (e.g., Manning, 2004; Scambelluri et al., 2015; Chen et al., 2016, 2020; Wang et al., 2017; Li et al., 2018), and therefore detectable Mg-isotopic variations might have been produced by reactions between mantle wedge and slab-derived fluids (Chen et al., 2016, 2020; Teng et al., 2016; Teng, 2017). The δ^{26}Mg values of Izu- and NEJ-arc rocks show co-variations with elemental and isotopic ratios suggestive of fluid addition (δ^{11}B and Nb/B; Fig. 6). We thus consider that the variation in δ^{26}Mg values in Izu and NEJ arc rocks are largely due to involvement of fluids derived from subducted slabs. Although δ^{11}B data are not available for SWJ rocks, their Nb/B ratios and δ^{26}Mg values are uncorrelated ($r^2 < 0.2$). A subducted slab consists of different lithologies (sediments, AOC, and ultramafic rocks), which contribute variably to the δ^{26}Mg signature of arc magmas. Below, the role of each lithology in the production of the δ^{26}Mg signature of arc magmas will be discussed.

5.3.1. Silicate-rich sediments and AOC

It is well known that subducted components, consisting of sediments, altered mafic rocks (denoted as altered oceanic crust or AOC), and altered ultramafic rocks (serpentinites), significantly contribute to the production of arc magmas (Schmidt and Poli, 1998).

Three different scenarios have been proposed for the addition of slab-derived components to sub-arc mantle; (1) AOC-derived aqueous fluid (e.g., Ishikawa and Nakamura, 1994), (2) AOC-derived melt (e.g., Pineda-Velasco et al., 2018), and (3) bulk sediment (e.g., Behn et al., 2011). We employ a simple binary mixing model for these scenarios. The modeling involves the assumption that magma sources beneath these arcs consist of the local mantle with fluids or melts of AOC, and melts or bulk materials of sediments. All parameters used in the modeling are listed in Supplementary Text S5 and Table S3, which include the mass fraction of sediment and AOC in the subducting slab, Mg-Sr elemental and isotope compositions of sub-arc mantle, sediment, and AOC. The results of the modeling are shown in Fig. 7a.

The carbonates and carbonate-rich sediments yield low δ^{26}Mg (−5.1 to −0.32 ‰; Fig. 1a; e.g., Huang and Xiao, 2016; Hu et al., 2017; Teng, 2017), and hence are potential to contribute to the light-δ^{26}Mg feature observed in some volcanic rocks from NEJ arc (Kampu; Fig. 3b). The contribution of carbonate-rich sediments will be discussed in Section 5.5. By contrast, silicate-rich sediments (e.g., clay) tend to have higher δ^{26}Mg values than the mantle (Fig. 1a; Teng et al., 2016; Hu et al., 2017), and hence they have the potential to produce a high-δ^{26}Mg feature in arc volcanic rocks. Analysis of Shimanto shales, an equivalent to terrigenous sediments subducted into the Nankai trench (Taira, 1988), support this

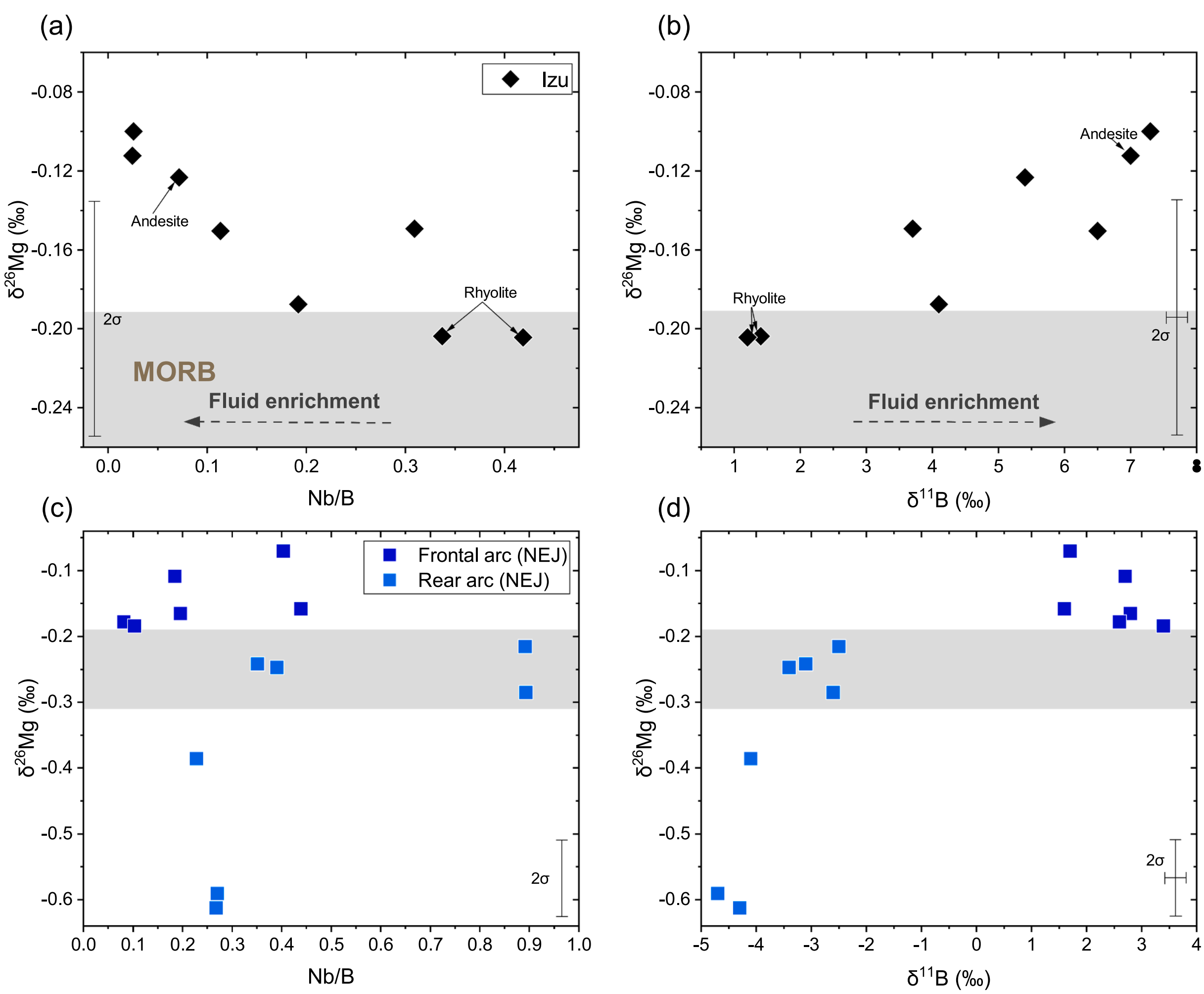

Fig. 6. The correlation between δ^{26}Mg values and Nb/B ratios and δ^{11}B of volcanic rocks from the Izu arc and NEJ. (a and b) δ^{26}Mg values versus Nb/B ratios and δ^{11}B, respectively, of volcanic rocks from the Izu arc. (c and d) δ^{26}Mg values versus Nb/B ratios and δ^{11}B, respectively, of volcanic rocks from the NE Japan arc. Uncertainty of δ^{26}Mg values for the studied samples is ± 0.06 ‰ and that of δ^{11}B values is ± 0.2‰ (2σ external reproducibility).

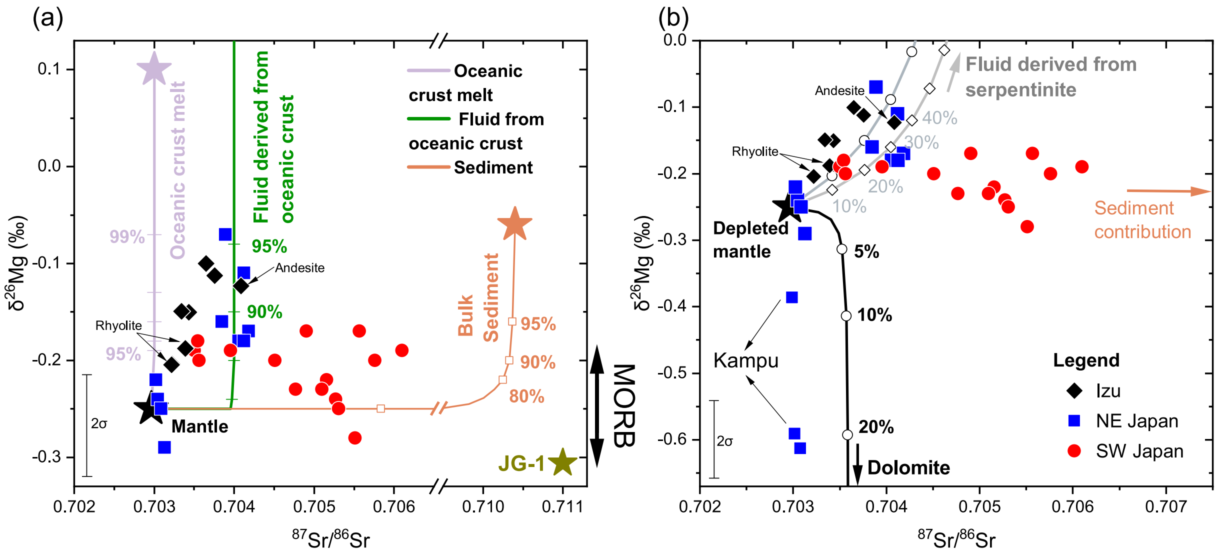

Fig. 7. (a) Results of modeling for δ^{26}Mg value and ^{87}Sr/^{86}Sr ratio of a magma source produced by mixing between the depleted mantle and bulk sediments (orange line), AOC-derived aqueous fluids (green line) and AOC-derived hydrous melt (purple line). (b) Results of modeling for δ^{26}Mg value and ^{87}Sr/^{86}Sr ratio of a magma source produced by mixing depleted mantle and serpentinite-derived fluids and dolomite. The δ^{26}Mg values of endmembers of serpentinite-derived fluids are assumed to be + 0.95 ‰ (open cycle symbol) and + 0.42 ‰ (open diamond symbol) by Chen et al., (2016) and Huang et al., (2020). See Table S3 for details about the parameters used for modeling. Uncertainty of δ^{26}Mg values for the studied samples is ± 0.06 ‰ (2σ external reproducibility).

idea; these sedimentary rocks have δ^{26}Mg values of −0.06 and −0.17 ‰ (Table 1 and S1). As the Mg isotope compositions of subducted sediments beneath NEJ and Izu arcs have not been reported, we use the highest value (−0.06 ‰) of the Shimanto shales as the approximate estimate of the subducted sediments beneath the Izu, NEJ, and SWJ arcs. The MgO (1.85 ± 0.59 wt%) of bulk sediments is calculated from the mean value of sediments from the Izu, Japan, and Nankai trenches (Plank, 2014). The trajectory of binary mixing between the local mantle and bulk sediments suggests that silicate-rich sediment-derived components cannot significantly shift the Mg isotope compositions of the sub-arc mantle to the high δ^{26}Mg values observed in our study unless the input of sediments is unrealistically high (> 95 %; orange line in Fig. 7a). It is also unlikely that sediment-derived melt could have significantly altered the Mg isotope composition of mantle peridotite as sediment melts also have low MgO contents [<0.6 wt%, calculated using MgO abundance of bulk sediment (1.85 wt%) with assumed melting degree of 30% (Pineda-Velasco et al., 2018) and partition coefficient of 4.4 (Johnson and Plank, 1999)]. Therefore, the addition of recycled silicate-rich sediments to the mantle source is unlikely to significantly alter δ^{26}Mg values of parental magmas for volcanic rocks in any arcs studied.

In the NEJ and Izu arc, slab-derived components are dominated by AOC-derived aqueous fluids (Ishikawa and Nakamura, 1994; Shibata and Nakamura, 1997; Moriguti and Nakamura, 1998; Taylor and Nesbitt, 1998). The MgO concentrations of AOC-derived fluids are estimated to be 1.12 wt% based on the solubility of Mg determined by an experimental study (Kessel et al., 2005). The δ^{26}Mg values of AOC range from −1.70 to +0.26 ‰, based on the analysis of seafloor basalts (Huang et al., 2015a, 2018; Wang et al., 2017). We chose the highest value of +0.26 ‰ among the analyses as the δ^{26}Mg value of AOC-derived fluids. Modeling results reveal that AOC-derived fluids are too poor in Mg to shift the Mg isotope composition of the mantle wedge (green line in Fig. 7a). Otherwise, a substantial amount of a fluid (95 wt% in a magma source) should be added to mantle in order to explain observed compositions in these arc rocks. If fluid-rock interaction occurs in an open system, mantle might be able to interact with a large quantity of fluid (the fluid-to-rock ratio is as high as 2; Hu et al., 2020). However, the interaction with a high fluid-to-rock ratio significantly modifies isotope compositions of other fluid-mobile elements such as Pb. Previous studies estimated a fluid-to-rock ratio in magma sources beneath these arcs as 0.01–0.05 (0.2–5% fluid in the source), which explains Pb isotopic compositions of volcanic rocks in these arcs (Taylor and Nesbitt, 1998; Kimura and Nakajima, 2014). Such a discrepancy is also found in the similar modeling for volcanic rocks in Lesser Antilles arc (Martinique) by Teng et al. (2016) who advocated the contribution of Mg-rich (and Pb-poor) fluids released from mafic/ultramafic lithologies with the subducted oceanic lithosphere. Considering that Pb (and Sr, Nd) in the slab-derived fluids in Izu arc are largely derived from AOC (Taylor and Nesbitt, 1998; Kimura and Nakajima, 2014), the source of Mg-rich fluids is considered to be slab lithologies other than AOC.

By contrast, the AOC beneath SWJ arc was suggested to have released fluids enriched in silicate components; i.e., melt (Kimura et al., 2014; Pineda-Velasco et al., 2018). The MgO concentrations (0.4 wt%) and δ^{26}Mg values (+0.1 ‰) of AOC-derived melts were taken from Wang et al. (2020), who estimated these values by considering isotope fractionation between melt and residual AOC under the condition for slab melting. The binary mixing between AOC melt and mantle (as its solid form) demonstrates that the δ^{26}Mg value of the mantle might not be significantly modified by AOC-derived melts unless an unrealistic AOC-melt to mantle ratio (>90 %) is assumed (purple line in Fig. 7a).

Collectively, our study suggested that fluids or melts derived from AOC and silicate-rich sediments have insignificant effects on Mg-isotopic features of arc magmas in Izu, NEJ, and SWJ. This is largely because these components have low Mg concentration (0.40–1.85 wt%; Table S3), compared with mantle peridotite (35–40 wt%; McDonough and Sun, 1995; Workman and Hart, 2005). As mentioned above, serpentinite could be a possible candidate for the source of high δ^{26}Mg fluids (Chen et al., 2016; Chen et al., 2020). The role of this component will be discussed in the next section.

5.3.2. Serpentinite

Serpentinites are characterized by high B abundance (up to 100 μg·g^{-1}) and high δ^{11}B value (+5.5 to +40.5 ‰; Marschall, 2018; Martin et al., 2020), compared to other constituents of a subducted slab (e.g., sediments and AOC; Ishikawa and Nakamura, 1994; Marschall, 2018) and mantle rocks (i.e., ultramafics; Marschall, 2018). Thus, B isotope compositions of arc magmas could be affected by serpentinite-derived fluids added to their sources (e.g., Cooper et al., 2020; Tonarini et al., 2007; Tonarini et al., 2011). Post-fluid addition processes include partial melting of a source and fractional crystallization of a parental magma, both of which do not significantly modify the B isotope composition inherited from the source (Ottolini et al., 2004). Serpentines are also major Mg carriers in a subducted slab, hence their roles in arc-magma production would be best constrained by B-Mg isotope systematics (e.g., Du et al., 2023).

An experimental study on a peridotite-fluid system suggested that fluids liberated from hydrous peridotite (MgO = 40.59 wt%) at sub-arc depths (4 GPa and 800 °C) could have the MgO abundance as high as 13–15 wt% [i.e., $D_{Mg}^{Fluid/hydrous\ peridotite} \approx 0.35$; Dvir et al. (2011)]. With the $D_{Mg}^{Fluid/hydrous\ peridotite}$ of 0.35 and MgO abundance of the subducted serpentinites [39.6 ± 2.6 wt%; Deschamps et al. (2013)], MgO content in serpentinite-derived fluids is calculated as 14 wt%. The estimated MgO abundance is comparable to that used in the previous study (e.g., MgO = 16.1 wt%; Huang et al., 2020).

For evaluating the effect of serpentinite-derived fluids in magmas in the NEJ, Izu, and SWJ arcs, a simple mass-balance modeling was employed. The MgO content for the fluid is assumed to be 14 wt% (see above). As the δ^{26}Mg value of serpentinite-derived fluids has not been reported so far, its δ^{26}Mg value is assumed to be +0.42 and +0.95 ‰ (Chen et al., 2016; Huang et al., 2020); the value is based on Mg isotope fractionation factor between magnesite and fluid (Schauble, 2011) and δ^{26}Mg values of magnesites and talc in serpentinized peridotite (Beinlich et al., 2014). For such modeling, the ^{87}Sr/^{86}Sr ratio is the best option to compare with the δ^{26}Mg value, as serpentinites are considered to have a significantly radiogenic ^{87}Sr/^{86}Sr ratio [~0.7051; Tonarini et al. (2007)] compared with pre-metasomatized mantle peridotite. The elemental and isotopic compositions of Sr of serpentinite-derived fluids are from Savov et al. (2005), Savov et al. (2007) and Tonarini et al. (2007), respectively (Table S3). Results of the modeling show that the addition of ~30–40 wt% serpentinite-derived ^{26}Mg-rich fluids to the mantle wedge is sufficient to explain the heavy Mg isotope compositions of samples at the frontal arc of the NEJ and Izu arcs (Fig. 7b). The estimated amounts of fluids are consistent with previous studies (Hu et al., 2020). The high fluid proportion (~0.3–0.4) estimated for these arcs could be reasonably achieved, if the fluid flow is focused or channelized in the mantle wedge (Pirard and Hermann, 2015; Huang et al., 2020). Presence of such a fluid flow is supported by U-series disequilibria (Yokoyama et al., 2003) and Li-isotope heterogeneity (Zhang et al., 2023) in arc volcanic rocks. The fluids would have ascent as a channelized flow and reached shallow and hot regions within the mantle wedge, where fluid-fluxed melting produced parental arc magmas (Grove and Till, 2019).

The lower-δ^{26}Mg values of rear-arc volcanic rocks are interpreted as a result of the decreasing contribution of serpentinite-derived fluids with increasing depths of a slab beneath in the NEJ and Izu arcs. The interpretation is consistent with the MORB-like δ^{11}B (Fig. 6b) and Nb/B ratios (Fig. 6a) of rear-arc rocks, compared with higher-than-MORB δ^{11}B and Nb/B ratios in frontal-arc rocks (Ishikawa and Nakamura, 1994). In SWJ, <20 wt% serpentinite-derived ^{26}Mg-rich fluids are estimated for magma sources of the arc magmas (Fig. 7b), which is also less than the contribution of this slab lithology to arc magmas from frontal arc regions in NEJ and Izu (20–30%). Note that the δ^{26}Mg values and ^{87}Sr/^{86}Sr ratios of SWJ arc rocks show an apparent decoupling, which is well explained by greater sediment contribution to the parental magmas of SWJ volcanic rocks (Feineman et al., 2013; Pineda-Velasco et al., 2018). In the next section, the source of the serpentinite-derived components and the possible cause for the different extents of serpentinite contributions to each arc will be discussed.

5.4. Source of serpentinite-derived components

Serpentinite mainly consists of serpentines and other phyllosilicates (e.g., talc and chlorite). It has been demonstrated that δ^{26}Mg values of different minerals in serpentinites show differences from each other (Fig. 1c). Dehydration of different hydrous phases with different δ^{26}Mg values might have produced fluids with variable δ^{26}Mg values (Li et al., 2018). Nevertheless, we first examine the feasibility of the production of high δ^{26}Mg components from subducted serpentinite.

Surface exposures of mantle wedge serpentinites include fore-arc mud volcanoes and exhumed subduction complexes. The δ^{26}Mg values of either type of serpentinites are indistinguishable from the mantle δ^{26}Mg value (–0.24 ± 0.05 ‰ for the former and –0.21 ± 0.08 ‰ for the latter; Li et al., 2018; Li et al., 2024; Wang et al., 2023). Abyssal serpentinites (unweathered) also have δ^{26}Mg values largely overlapping with the mantle δ^{26}Mg value (–0.19 ± 0.07 ‰; Liu et al., 2017). Accordingly, it has been generally considered that significant Mg isotope fractionation does not occur during serpentinization (Fig. 1c; Beinlich et al., 2014). However, recent studies have documented high δ^{26}Mg values in serpentinites from ophiolites (to +0.96 ‰; de Obeso et al., 2021; Zhao et al., 2023) and in high-pressure metamorphic rocks (to +0.29 ‰; Chen et al., 2020). It is therefore still premature to conclude that serpentinites in mantle wedge have homogeneous δ^{26}Mg values similar to that of unaltered MORB.

Extensively altered peridotites contain talc that was formed via reactions of serpentinite and aqueous or carbonate-bearing fluids (Beinlich et al., 2014; Li et al., 2018). Such reactions induce significant isotope fractionation of Mg, possibly increasing the δ^{26}Mg value by 0.1–0.3 ‰ (talc: +0.06 to +0.30 ‰; Fig. 1c). High-δ^{26}Mg features have been found in talc-bearing metaperidotites from Francisco Complex (Li et al., 2018). Moreover, hydrous minerals with high δ^{26}Mg values in exhumed subduction complexes are considered to have formed via infiltration of fluids from talc-bearing metaperidotites [Alps (Chen et al., 2016; Chen et al., 2020), and Tianshan (Wang et al., 2017)].

Pogge von Strandmann et al. (2015) showed that chlorites with low δ^{26}Mg values of −0.38 to −0.24 ‰ occurred in a mélange (metabasalt and serpentinite hybrid rock; Fig. 1c), which was exhumed from the slab-mantle interface at sub-arc depths (55–75 km). However, its Mg isotope feature (i.e., apparently low-δ^{26}Mg value) might be attributed to diffusive isotope fractionation. Thus, a representative δ^{26}Mg value of chlorite in sub-arc serpentinites is not available from the existing studies. Instead, Deng et al. (2024) calculated that the fluids released by the breakdown of chlorite are significantly enriched in heavier Mg isotopes (by +0.66 ‰ in δ^{26}Mg). In summary, subducted serpentinites beneath an arc potentially have δ^{26}Mg values higher than normal mantle, owing to the possible existence of high δ^{26}Mg minerals including antigorite, chlorite, and talc.

Given that serpentinites are metamorphic rocks of ultramafic protoliths, they are considered to occur in the mantle section of a subducted slab and the lowermost part of mantle wedge (Deschamps et al., 2013). Both types of serpentinites subduct into sub-arc depths and release fluids that metasomatize the overlying mantle wedge (Savov et al., 2005, 2007; Ribeiro and Lee, 2017). The high B/Nb ratios and δ^{11}B values of arc volcanic rocks are also consistent with the contributions of serpentinite-derived fluids to their mantle sources (e.g., De Hoog and Savov, 2018; Xiong et al., 2022). However, it is difficult to distinguish the contributions from either serpentinite to arc magmas solely by geochemical and isotope studies (Cooper et al., 2020; Rojas-Kolomiets et al., 2023). We thus attempt to provide an argument for the roles of these serpentinites by combining the thermal structures (*P-T* path) of subduction zones beneath the arcs (van Keken and Wilson, 2023).

Talc, chlorite, and serpentine (antigorite) are stable until it is heated to *c*. 600–800 °C at depths of 90–160 km (Spandler et al., 2008). The mantle section in a subducted slab (slab mantle) beneath volcanoes in SWJ (105±15 km) and that beneath frontal arc regions in NEJ and Izu (130–160 km) have temperatures estimated around 600–650 °C and 400–500 °C, respectively (Fig. 8a; Syracuse et al., 2010). In either arc, slab mantles beneath these volcanoes have temperatures lower than temperatures for the breakdown of talc, chlorite, and antigorite (Fig. 8a). In contrast, mantle wedge serpentinites beneath the frontal arc of the NEJ and Izu arcs have temperatures of 770–800 °C, being well within the range of temperatures for the breakdown of talc and chlorite

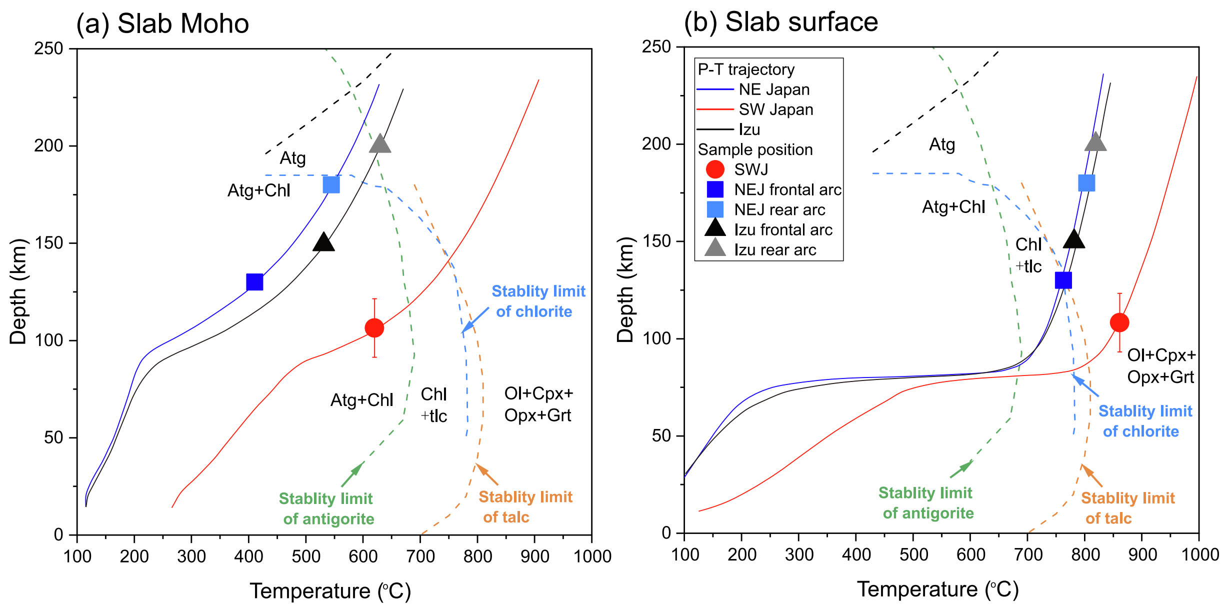

Fig. 8. *P-T* paths of (a) lithospheric mantle (slab Moho) and (b) surface of the subducting slab beneath Izu, NEJ, and SWJ arcs. The temperatures of the slab surface and slab Moho are assumed to represent those of mantle wedge serpentinite and slab lithosphere serpentinite, respectively. The stability limits of hydrous minerals (talc, chlorite, and antigorite) are from Spandler et al. (2008; references therein). The slab *P-T* path from van Keken and Wilson (2023) is applied. The calculation method of this model was modified based on the D80 model of Syracuse et al. (2010). As SWJ experienced the slab tearing and distortion processes, actual WBZ depth cannot be precisely constrained. Therefore, we applied the average value of estimated slab depth (105 km) with an error bar (±15 km).

(750–800 °C; Fig. 8b). Therefore, mantle wedge serpentinite, rather than slab serpentinite, could supply fluids that have dominantly contributed to high-δ^{26}Mg signatures to sub-arc mantle beneath all of the studied arcs. It is however noted that we do not rule out the dehydration of serpentinites within a subducting slab; rather it should have occurred in most subduction zones, revealed by intra-slab seismicity (Peacock, 2001), subduction thermal model (Hyndman and Peacock, 2003) and subduction metamorphic petrology (Scambelluri et al., 2001).

Rear-arc volcanic rocks in NEJ (except Kampu) and Izu arc exhibit MORB-like δ^{26}Mg values (Fig. 3a and b). Such a feature implies that talc and chlorite in mantle wedge serpentinite were completely broken down while it was dragged down to the rear-arc depths with temperature > 820 °C (Fig. 8b). In SWJ, the MORB-like δ^{26}Mg values suggested that the fluid fraction derived from mantle wedge serpentinite added to the mantle source is significantly lower than those estimated for NEJ and Izu (frontal-arc regions). The smaller contribution of fluids from mantle wedge serpentinite could be attributed to the higher *T/P* gradient in the SWJ subduction zone (Peacock and Wang, 1999). Mantle wedge serpentinites beneath SWJ have temperatures of around 850 °C, which is 50–100 °C higher than the temperatures for the breakdown of talc and chlorite (750–800 °C; Fig. 8b; Syracuse et al., 2010). The swift rise of temperature might have led to the rapid decomposition of hydrous minerals in mantle wedge serpentinite. Therefore, the Mg isotope composition of arc magma beneath SWJ recorded less but variable contribution from serpentinite-derived fluids, compared to those in NEJ and the Izu arc.

5.5. *Carbonate as a possible low-δ^{26}Mg component*

Volcanic rocks from Kampu, located in the rear arc of NEJ, exhibit lighter Mg isotopic compositions (δ^{26}Mg = –0.61 and –0.39 ‰) than unaltered MORB (or mantle; Fig. 9), and other arc volcanic rocks from modern subduction zones (Fig. 1b), but similar to the <110 Ma intra-continental basalts from eastern China (−0.60 to 0.30 ‰; Fig. 9; Yang et al., 2012; Huang et al., 2015b; Li et al., 2017). Similar low-δ^{26}Mg features from subduction systems have been only reported from volcanic rocks and ultramafic massif (exhumed complex) from continental collision zones, located in the inland of China (Shen et al., 2018; Tian et al., 2018). It is therefore noted that our case is the first example of the occurrence of low-δ^{26}Mg volcanic rocks from modern arc systems.

Four scenarios have been proposed for the production of low-δ^{26}Mg mantle-derived magmas: (1) accumulation of ilmenite enriched in light Mg isotopes (Sedaghatpour et al., 2013), (2) fractionation of chromite and titanomagnetite enriched in heavy Mg isotopes (Su et al., 2017, 2019; Wang et al., 2021), (3) assimilation of crust rocks metasomatized by low-δ^{26}Mg carbonate fluids (Yang et al., 2016), and (4) recycling of subducted low-δ^{26}Mg carbonates (e.g., Huang et al., 2015b; Li et al., 2017; Tian et al., 2018; Tan et al., 2022).

The first and second scenarios are excluded as discussed in Section 5.2.1. The interaction of mantle-derived parental magmas and lower-crustal mafic rocks was suggested for the Kampu volcano (Yamamoto et al., 2013). However, the lower crustal xenoliths, found in the vicinity, do not contain carbonates (Yamamoto et al., 2013). Hence, the third scenario could also be ruled out. We thus consider that the involvement of carbonates occurred at greater depths, i.e., in the source regions of mantle-derived magmas.

Distinctive geochemical features of Kampu volcanic rocks, characterized by higher Li/Y, La/Sm, Th/Nb, and U/Nb ratios than other NE-Japan volcanic rocks, were first noted by Moriguti et al. (2004). They attributed such features to the addition of slab-derived via the breakdown of lawsonite at a depth of 180 km. It is however considered that lawsonite breakdown hardly explains the low-δ^{26}Mg feature of Kampu volcanic rocks, because fluids released from (Mg-free) lawsonite should have little Mg. We thus consider that other minerals played a role in the production of the low δ^{26}Mg feature of Kampu volcanic rocks.

Carbonates subducted with oceanic lithosphere beneath arc volcanoes are included in sediments and AOC. These carbonates would have been formed as precipitates from seawater (biogenic) or secondary minerals by seawater-rock interaction (non-biogenic). Regardless of their origins, they generally have high abundances of P, Sr, and U, and are enriched in LREE (relative to HREE) and depleted in HFSE (Veizer, 1983; Staudigel et al., 1996; Kelley et al., 2005). The Kampu volcanic rocks have higher abundances of P_2O_5 (0.34–0.37 wt%), Sr (848–874 $\mu g\cdot g^{-1}$) and U (1.51–1.92 $\mu g\cdot g^{-1}$) than other NEJ volcanic rocks ([P_2O_5] = 0.04–0.26 wt%, [Sr] = 160–581 $\mu g\cdot g^{-1}$, [U] = 0.06–1.17 $\mu g\cdot g^{-1}$; Supplementary Table S1). They also have higher U/Nb ratios and lower

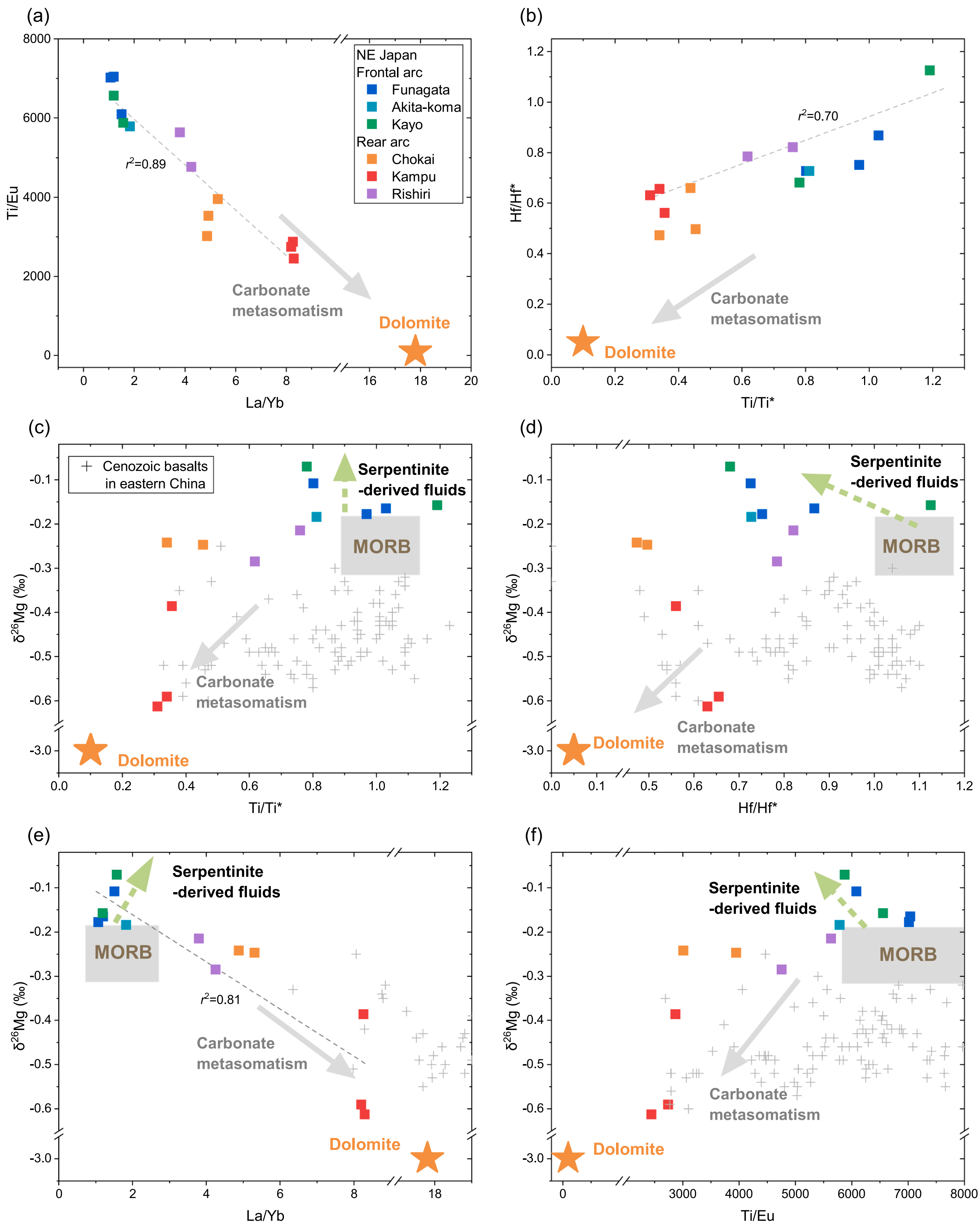

Fig. 9. Variations of (a) La/Yb versus Ti/Eu, (b) Ti/Ti* versus Hf/Hf*, and (c) Ti/Ti*, (d) Hf/Hf*, (e) La/Yb, and (f) Ti/Eu versus δ^{26}Mg values for the volcanic rocks from NEJ arc. Two series of volcanic rocks, one from the frontal arc and another rear arc of the arc, display Mg isotopic and major- and trace-element compositional dichotomy. Elemental anomalies are calculated as follows: $Ti/Ti^* = Ti_N/(Sm_N^{-0.055} \times Nd_N^{0.333} \times Gd_N^{0.722})$, $Hf/Hf^* = Hf_N/(Sm_N \times Nd_N)^{0.5}$, where the subscript N means normalized to the primitive mantle (Sun and McDonough, 1989). Mg isotopic composition ($\delta^{26}Mg = -0.25 \pm 0.06$ ‰) and other elemental properties of MORB are from Hofmann (1988) and Teng et al. (2010a). The Mg isotopic composition and other elemental properties of dolomite are from Wang et al. (2014), Higgins et al. (2018), and Tian et al. (2018). Data sources for the Cenozoic basalts in eastern China are from Li et al. (2017 and references therein).

Ti/Eu, Ti/Ti*, and Hf/Hf* ratios, compared with other NEJ volcanic rocks (Fig. 9; Moriguti et al., 2004). These features are considered to be consistent with the derivation of Kampu magmas by melting of sources that have carbonate components (Fig. 9).

Thermodynamic modeling predicted that subducted carbonates could be dissociated (decarbonation) in the depth of arc volcanoes (80–180 km) if fluids are sufficiently infiltrated from external sources (Kerrick and Connolly, 2001). Considering the subduction *P-T* paths, other slab lithologies (AOC and slab mantle) should have dehydrated at these depths beneath NE Japan, having resulted in fluid-mediated decarbonation in the slab. Whereas slab decarbonation is considered to have not occurred beneath SW Japan due to the high *T/P* gradient of the subducting slab (Gorce et al., 2019). Decarbonation reaction produces fluids containing significant amounts of CO_2 (Kerrick and Connolly, 2001). Such fluids infiltrate into the overlying mantle, resulting in a significant drop of the solidus of the subarc (90–100 km) mantle (Wendlandt and Mysen, 1980).

The δ^{26}Mg values of NEJ volcanic rocks are negatively correlated with their La/Yb ratios (r^2=0.81; Fig. 9e). The variation in La/Yb ratio could be attributed to (1) the variation in residual source mineralogy (garnet facies vs spinel facies), (2) chemical heterogeneity of magma sources, and (3) varying degree of melting of a common source. Scenario 1 is ruled out by the discussion in Section 5.2.2; the sources of NE-Japan volcanic rocks are considered to be dominated by spinel-facies peridotites. A melt from a garnet-facies source should have a higher La/Yb ratio and high δ^{26}Mg value (discussed above); this is not the case for NE Japan (high La/Yb rocks have low δ^{26}Mg values). Scenario 2 is also unlikely, as the mantle wedge beneath NE Japan is considered to be homogeneous in terms of REE compositions (Sakuyama and Nesbitt, 1986; Shibata and Nakamura, 1997).

The extent of melting of a magma source beneath NEJ arc decreases from frontal-arc regions (F = 20%) to rear-arc regions (F = 5%), due to an increase in melting depth across the arc (Sakuyama and Nesbitt, 1986). The Kampu volcano is located in a back-arc region, and the high La/Yb ratios of the Kampu rocks are considered to be partly due to the smaller degree of melting of the source. Volcanic rocks from other rear-arc volcanoes (Chokai and Rishiri) also have higher La/Yb ratios and slightly lower δ^{26}Mg values than the frontal-arc rocks. Accordingly, a negative correlation between the La/Yb ratio and δ^{26}Mg value in NEJ rocks is observed. Owing to the difficulty in constraining the compositions of subducted carbonate sediments and magma sources (mantle wedge), it is quite difficult to quantitatively estimate the relative contributions of melting processes and source enrichments (carbonate inputs) to the variation in La/Yb ratios in NEJ volcanic rocks.

We employed mass balance calculation to examine the mass fraction of sediment that was incorporated into a magma source for the parental magma of Kampu volcanic rocks. For the modeling, the species of subducted carbonate and its elemental and isotopic composition should be constrained in advance. Carbonates in sediments prior to subduction might be dominated by Ca-rich carbonates (Plank and Langmuir, 1998). Subordinate amounts of Mg-rich carbonates (dolomite) might also occur in sediments as a product of carbonate diagenesis (Higgins et al., 2018). Subducted carbonates might also include Mg-rich carbonates, which are formed by Ca-Mg exchange between Ca-rich carbonates and mafic minerals in adjacent mafic or ultramafic rocks during subduction metamorphism (Yaxley and Green, 1994). The δ^{26}Mg values of shallow, diagenetic Mg-rich carbonates are reported to be c. –3 ‰ (Higgins et al., 2018; Liu et al., 2024). For deep, metamorphic Mg-rich carbonates, similar δ^{26}Mg values (–3 to –2 ‰) are estimated from the analysis of ultrahigh-pressure metamorphic marbles (Wang et al., 2014). Therefore, we used the δ^{26}Mg value of –3 ‰ for the subducted carbonate (dolomite) in the modeling, although the process responsible for its low-δ^{26}Mg feature is not well constrained.

A simple binary mixing between mantle wedge and dolomite was performed for a δ^{26}Mg-^{87}Sr/^{86}Sr system (Fig. 7b). The MgO concentration (22 wt%) and δ^{26}Mg value (–3 ‰; Wang et al., 2014; Higgins et al., 2018) of dolomite are from its chemical formula and the above discussion. Whereas the Sr content (0.7036) and ^{87}Sr/^{86}Sr ratio (1800 μg·g^{-1}) of dolomite is from Romer et al. (2003) and Wawrzenitz et al. (2019). Our results suggest that <20% of dolomites were incorporated into the mantle source of Kampu parental magma. The estimated mass fraction of carbonates corresponds to CO_2 of <10 wt%. Carbonate dissociation released CO_2 which has been incorporated into mantle. Hence the melting would have occurred under the condition at which CO_2 is present. Under relatively low-pressure conditions (<3 GPa), the melting of a source with <10 wt% CO_2 (together with H_2O) could produce subalkaline basaltic magmas (Wendlandt and Mysen, 1980), consistent with the silica-saturated features of the Kampu volcanic rocks.

6. Implications

As discussed in the preceding section, Mg isotopic signatures in magmatic rocks from the NEJ, SWJ, and Izu arcs could be explained by the contribution of fluids derived from mantle wedge serpentinite and carbonate (Fig. 10). The thermal structure and slab depths might control the Mg isotope variations in global subduction zone magmas. The breakdown and dehydration of serpentinite minerals (e.g., antigorite, chlorite, and talc) occurs at frontal-arc depths in cold subduction zones and produces isotopically-heavy-Mg fluids (Fig. 10a). By contrast, in warm subduction zones, major serpentinite minerals break down at depths shallower than sub-arc slab depth (Fig. 10b). Therefore, serpentinite signatures (high δ^{26}Mg values) cannot be transported into the sub-arc mantle and arc magmas under such conditions. At this stage, the solubility of Ca-rich carbonate (i.e., calcite) is significantly higher than those of dolomite and magnesite based on molecular dynamics (Pan et al., 2013); thus, dissolved carbonate components in dehydrated fluid have abundant Ca but little Mg, which has a limited influence on the Mg isotope composition of the mantle wedge (Li et al., 2017).

Beyond frontal-arc depths, hydrous minerals (e.g., antigorite, chlorite and talc) with heavy Mg isotopic signature might have been broken down completely (Ulmer and Trommsdorff, 1995; Peacock and Wang, 1999), resulting in the production of parental magmas of rear-arc volcanic rocks with MORB-like Mg isotopic signatures in cold subduction zones (Fig. 10a). Nevertheless, lower-than-MORB δ^{26}Mg values are found in volcanic rocks in some rear-arc regions (such as that in NEJ arc and Tengchong volcano; Tian et al., 2018). Our study demonstrates that such a feature could be explained by subducted Mg-rich carbonates (dolomite). Across-arc variations in δ^{26}Mg values in other arcs might also result from a combined effect of serpentinite and carbonate subduction.

7. Conclusion

Volcanic rocks from the frontal arc region of NEJ and Izu have isotopically heavy Mg, compared to the mantle-like or isotopically light Mg isotope signatures of those from SWJ and the rear arc of NEJ and Izu. Possible causes of Mg-isotopic variability are examined, and we conclude:

1. The recycling of silicate-rich sediments, AOC, and slab serpentinites has no salient effects on the Mg isotope compositions of volcanic rocks from the Izu, NEJ, and SWJ arcs.
2. The high δ^{26}Mg values of volcanic rocks from the frontal arc might be generated by the fluid from mantle wedge serpentinite in channelized flow.
3. The MORB-like δ^{26}Mg signature in volcanic rocks from rear-arc depths and hot arcs indicates the complete breakdown of serpentinite minerals (e.g., antigorite, chlorite, and talc).
4. The dehydration of mantle wedge serpentinite in different *P-T* conditions exerts a strong control on within-arc and inter-arc Mg isotope variations in global subduction zone magmas.

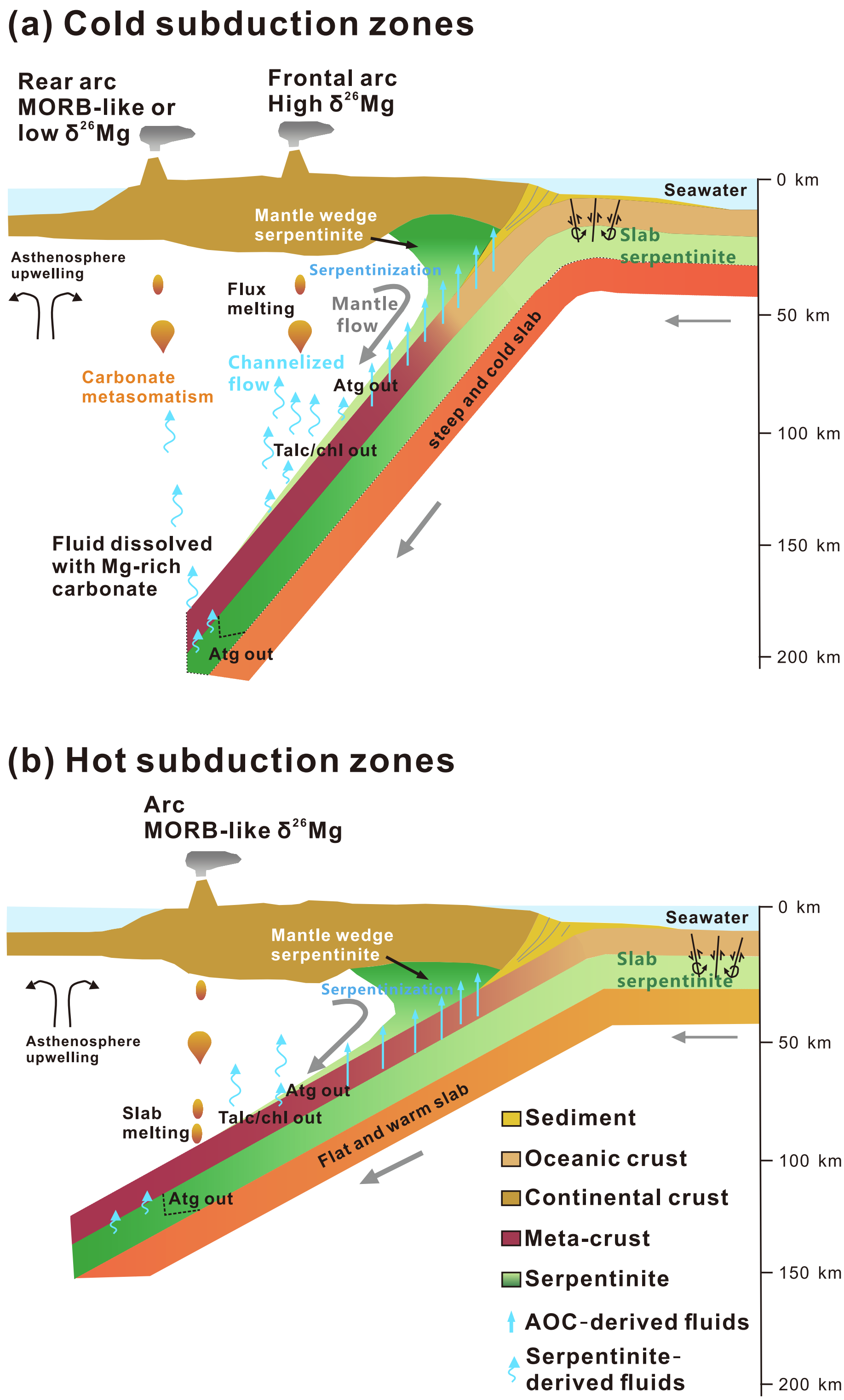

Fig. 10. Schematic of the models depicting the intra-arc and inter-arc variations in Mg isotope compositions of volcanic rocks from the NEJ, SWJ, and Izu subduction zones, caused by various contributions of subducted serpentinites and carbonates (Modified from Pagé and Hattori, 2019). (a) In cold subduction zones, the mantle wedge serpentinite is dehydrated and releases fluids that migrate upward in channelized flow. Production of high-δ^{26}Mg magmas is confined in frontal arc regions, as carrier phases of heavy Mg isotopes break down at slab depths beneath these regions. In some rear-arc regions (such as NEJ arc), δ^{26}Mg values that are lower than mantle are found in volcanic rocks, which might result from the melting of the source metasomatized by fluids from subducted Mg-rich carbonates (i.e., dolomite). (b) In warm subduction zones, hydrous minerals [e.g., talc, chlorite (chl), and antigorite (Atg)] in mantle wedge serpentinite break down at shallower depths (<100 km), and mantle melting might be induced by the influx of low-Mg hydrous silicate melts from sediments or AOC (Pineda-Velasco et al., 2018). Accordingly, Mg isotope signatures in arc magmas are dominantly inherited from mantle wedge (i.e., MORB-like δ^{26}Mg).

5. The presence of a light Mg isotopic composition in some volcanic rocks from rear arc regions indicates that Mg-rich carbonate could be transferred into the deep mantle wedge at rear-arc depths of 150–400 km in subduction zones.

CRediT authorship contribution statement

Wei Zhang: Writing – review & editing, Writing – original draft, Project administration, Methodology, Investigation, Formal analysis, Data curation, Conceptualization. **Hiroshi Kitagawa:** Writing – review & editing, Visualization, Supervision, Project administration, Investigation, Conceptualization. **Fang Huang:** Writing – review & editing, Validation, Supervision.

Data availability

Data are available through figshare at https://doi.org/10.6084/m9.figshare.26095108.v7.

Declaration of competing interest

The authors declare that they have no known competing financial interests or personal relationships that could have appeared to influence the work reported in this paper.

Acknowledgements

The authors would like to thank members of the Pheasant Memorial Laboratory for their support in the laboratory and Dr. Yi-Xiang Chen, Ding-Sheng Jiang, and Xiao-Ning Liu for their helpful suggestions in the discussion. Yoshiyuki Tatsumi and Tetsumaru Itaya are thanked for donating Izu-arc volcanic rocks and Shimanto shales, respectively. We also thank Christian Potiszil for improving the initial manuscript. We are also grateful for reviews by Kwan-Nang Pang and three anonymous reviewers and for editorial handling by Shichun Huang and Jeffrey G. Catalano. Financial support for this project was provided by National Natural Science Foundation of China (Grant Number 42403003), China Postdoctoral Science Foundation (Grant Number 2023M743359), JST SPRING (Grant Number JPMJSP2126, Japan), and Program for Promoting the Enhancement of Research University by MEXT, Japan.

Appendix A. Supplementary material

The material includes texts for petrographic descriptions of the studied samples (volcanic rocks from Izu, NE-Japan and SW-Japan arcs), a method for analyzing major-element compositions of the Izu samples, geochemical methods for evaluating post-eruptive alteration and pre-eruptive magmatic processes (fractional crystallization and partial melting), a review of the previous studies relevant to an effect of crustal assimilation on SW-Japan magmas, parameters used for the modelings of partial melting of and mixing of end-member components in magma sources, figures of photomicrographic images and across-arc variations of the differentiation index of the samples, and tables of major- and trace-element and Sr-Nd-Pb-B-Li isotope compositions of the samples and parameter lists for the modelings of partial melting of and mixing of end-member components in magma sources. Supplementary material to this article can be found online at https://doi.org/10.1016/j.gca.2024.12.024.

References

Ando, A., Kamioka, H., Terashima, S., Itoh, S., 1989. 1988 values for GSJ rock reference samples, "Igneous rock series". Geochem. J. 23, 143–148.
Aoki, Y., Tsunematsu, K., Yoshimoto, M., 2019. Recent progress of geophysical and geological studies of Mt. Fuji Volcano. Japan. Earth Sci. Rev. 194, 264–282.
Araoka, D., Yoshimura, T., 2019. Rapid purification of alkali and alkaline-earth elements for isotope analysis (δ ^{7}Li, δ^{26}Mg, ^{87}Sr/^{86}Sr, and δ ^{88}Sr) of rock samples using borate fusion followed by ion chromatography with a fraction collector system. Anal. Sci. 35, 751–757.
Babechuk, M.G., Widdowson, M., Kamber, B.S., 2014. Quantifying chemical weathering intensity and trace element release from two contrasting basalt profiles, Deccan Traps. India. Chem. Geol. 363, 56–75.
Baker, P.A., Burns, S.J., 1985. Occurrence and formation of dolomite in organic-rich continental margin sediments. AAPG Bull. 69, 1917–1930.
Bebout, G.E., 2007. Metamorphic chemical geodynamics of subduction zones. Earth Planet. Sci. Lett. 260, 373–393.
Behn, M.D., Kelemen, P.B., Hirth, G., Hacker, B.R., Massonne, H., 2011. Diapirs as the source of the sediment signature in arc lavas. Nat. Geosci. 4, 641–646.
Beinlich, A., Mavromatis, V., Austrheim, H., Oelkers, E.H., 2014. Inter-mineral Mg isotope fractionation during hydrothermal ultramafic rock alteration – Implications for the global Mg-cycle. Earth Planet. Sci. Lett. 392, 166–176.
Boschi, C., Bonatti, E., Ligi, M., Brunelli, D., Cipriani, A., Dallai, L., D'Orazio, M., Früh-Green, G.L., Tonarini, S., Barnes, J.D., Bedini, R.M., 2013. Serpentinization of mantle peridotites along an uplifted lithospheric section, Mid Atlantic Ridge at 11° N. Lithos 178, 3–23.
Brewer, A.W., Teng, F., Mullen, E., 2018. Magnesium isotopes as a tracer of crustal materials in volcanic arc magmas in the northern Cascade Arc. Front. Earth Sci. 6, 21.
Cannaò, E., Malaspina, N., 2018. From oceanic to continental subduction; implications for the geochemical and redox evolution of the supra-subduction mantle. Geosphere 14, 2311–2336.
Chen, Y., Schertl, H., Zheng, Y., Huang, F., Zhou, K., Gong, Y., 2016. Mg–O isotopes trace the origin of Mg-rich fluids in the deeply subducted continental crust of Western Alps. Earth Planet. Sci. Lett. 456, 157–167.
Chen, Y., Demény, A., Schertl, H., Zheng, Y., Huang, F., Zhou, K., Jin, Q., Xia, X., 2020. Tracing subduction zone fluids with distinct Mg isotope compositions: Insights from high-pressure metasomatic rocks (leucophyllites) from the Eastern Alps. Geochim. Cosmochim. Acta 271, 154–178.
Cooper, G.F., Macpherson, C.G., Blundy, J.D., Maunder, B., Allen, R.W., Goes, S., Collier, J.S., Bie, L., Harmon, N., Hicks, S.P., Iveson, A.A., Prytulak, J., Rietbrock, A., Rychert, C.A., Davidson, J.P., the VoiLA team, 2020. Variable water input controls evolution of the Lesser Antilles volcanic arc. Nature 582, 525–529.
De Hoog, J.C., Savov, I.P., 2018. Boron isotopes as a tracer of subduction zone processes. In: Marschall, H., Foster, G. (Eds.), *Boron Isotopes: the Fifth Element*. Springer, Cham, pp. 217–247.
de Obeso, J.C., Santiago Ramos, D.P., Higgins, J.A., Kelemen, P.B., 2021. A Mg isotopic perspective on the mobility of magnesium during serpentinization and carbonation of the Oman ophiolite. J. Geophys. Res. Solid Earth 126, e2020JB020237.
Defant, M.J., Drummond, M.S., 1990. Derivation of some modern arc magmas by melting of young subducted lithosphere. Nature 347, 662–665.
Deng, X., Chen, Y., Wang, W., Li, Y., Xiao, Z., Wu, Z., 2024. Heavy magnesium isotopic signatures in arc lavas might be attributed to dehydration of subducting hydrated mantle. Commun. Earth Environ. 5, 299.
Deschamps, F., Godard, M., Guillot, S., Hattori, K., 2013. Geochemistry of subduction zone serpentinites: A review. Lithos 178, 96–127.
Du, L., Zhang, Y., Zhu, H., Zhang, Z., An, Y., Yuan, C., Huang, Z., Li, X., Long, X., 2023. Different effects of serpentinite-derived and slab-derived fluids on arc magmatism in the Chinese Eastern Tianshan: evidence from Mg–B isotopic systematics. J. Geol. Soc. Lond. 180 jgs2023-011.
Duan, H., Yang, B., Huang, F., 2023. Site-specific isotope effect: Insights from equilibrium magnesium isotope fractionation in mantle minerals. Geochim. Cosmochim. Acta 357, 13–25.
Dvir, O., Pettke, T., Fumagalli, P., Kessel, R., 2011. Fluids in the peridotite–water system up to 6 GPa and 800 °C: new experimental constrains on dehydration reactions. Contrib. Mineral. Petrol. 161, 829–844.
Evans, B.W., Hattori, K., Baronnet, A., 2014. Serpentinite: What, Why, Where? Elements 9, 99–106.
Feineman, M., Moriguti, T., Yokoyama, T., Terui, S., Nakamura, E., 2013. Sediment-enriched adakitic magmas from the Daisen volcanic field, Southwest Japan. Geochem. Geophys. Geosyst. 14, 3009–3031.
Fram, M.S., Lesher, C.E., Volpe, A.M., 1998. Mantle melting systematics: transition from continental to oceanic volcanism on the southeast Greenland margin. Proceedings of the Ocean Drilling Program, Scientific Results 152.
Fujinawa, A., 1988. Tholeiitic and calc-alkaline magma series at Adatara volcano, northeast Japan: 1. Geochemical Constraints on Their Origin. Lithos 22, 135–158.
Galy, A., Yoffe, O., Janney, P.E., Williams, R.W., Cloquet, C., Alard, O., Halicz, L., Wadhwa, M., Hutcheon, I.D., Ramon, E., 2003. Magnesium isotope heterogeneity of the isotopic standard SRM980 and new reference materials for magnesium-isotope-ratio measurements. J. Anal. at. Spectrom. 18, 1352–1356.
Gorce, J.S., Caddick, M.J., Bodnar, R.J., 2019. Thermodynamic constraints on carbonate stability and carbon volatility during subduction. Earth Planet. Sci. Lett. 519, 213–222.
Grove, T.L., Till, C.B., 2019. H_2O-rich mantle melting near the slab-wedge interface. Contrib. Mineral. Petrol. 174, 80.
Higgins, J.A., Blättler, C.L., Lundstrom, E.A., Santiago-Ramos, D.P., Akhtar, A.A., Ahm, A.-S.-C., Bailik, O., Holmden, C., Bradbury, H., Murray, S.T., Swart, P.K., 2018. Mineralogy, early marine diagenesis, and the chemistry of shallow-water carbonate sediments. Geochim. Cosmochim. Acta 220, 512–534.
Hofmann, A.W., 1988. Chemical differentiation of the Earth: the relationship between mantle, continental crust, and oceanic crust. Earth Planet. Sci. Lett. 90, 297–314.
Hu, Y., Teng, F., Plank, T., Huang, K., 2017. Magnesium isotopic composition of subducting marine sediments. Chem. Geol. 466, 15–31.

Hu, Y., Teng, F., Ionov, D.A., 2020. Magnesium isotopic composition of metasomatized upper sub-arc mantle and its implications to Mg cycling in subduction zones. Geochim. Cosmochim. Acta 278, 219–234.
Huang, J., Ke, S., Gao, Y., Xiao, Y., Li, S., 2015a. Magnesium isotopic compositions of altered oceanic basalts and gabbros from IODP site 1256 at the East Pacific Rise. Lithos 231, 53–61.
Huang, J., Li, S., Xiao, Y., Ke, S., Li, W., Tian, Y., 2015b. Origin of low δ^{26}Mg Cenozoic basalts from South China Block and their geodynamic implications. Geochim. Cosmochim. Acta 164, 298–317.
Huang, J., Guo, S., Jin, Q., Huang, F., 2020. Iron and magnesium isotopic compositions of subduction-zone fluids and implications for arc volcanism. Geochim. Cosmochim. Acta 278, 376–391.
Huang, K.J., Teng, F.Z., Wei, G.J., Ma, J.L., Bao, Z.Y., 2012. Adsorption-and desorption-controlled magnesium isotope fractionation during extreme weathering of basalt in Hainan Island, China. Earth Planet. Sci. Lett. 359, 73–83.
Huang, K., Teng, F., Plank, T., Staudigel, H., Hu, Y., Bao, Z., 2018. Magnesium isotopic composition of altered oceanic crust and the global Mg cycle. Geochim. Cosmochim. Acta 238, 357–373.
Huang, J., Xiao, Y., 2016. Mg-Sr isotopes of low-δ^{26}Mg basalts tracing recycled carbonate species: Implication for the initial melting depth of the carbonated mantle in Eastern China. Int. Geol. Rev. 58, 1350–1362.
Hunter, A.G., Blake, S., 1995. Petrogenetic evolution of a transitional tholeiite–calc-alkaline series: Towada volcano. Japan. J. Petrol. 36, 1579–1605.
Hyndman, R.D., Peacock, S.M., 2003. Serpentinization of the forearc mantle. Earth Planet. Sci. Lett. 212, 417–432.
Ishida, M., 1992. Geometry and relative motion of the Philippine Sea plate and Pacific plate beneath the Kanto-Tokai district, Japan. J. Geophys. Res. Solid Earth 97, 489–513.
Ishikawa, T., Nakamura, E., 1994. Origin of the slab component in arc lavas from across-arc variation of B and Pb isotopes. Nature 370, 205–208.
Ishizuka, O., Taylor, R.N., Milton, J.A., Nesbitt, R.W., Yuasa, M., Sakamoto, I., 2006. Variation in the mantle sources of the northern Izu arc with time and space – Constraints from high-precision Pb isotopes. J. Volcanol. Geotherm. Res. 156, 266–290.
Jahn, B., 2010. Accretionary orogen and evolution of the Japanese Islands: Implications from a Sr-Nd isotopic study of the Phanerozoic granitoids from SW Japan. Am. J. Sci. 310, 1210–1249.
Johannes, W., 1984. Beginning of melting in the granite system Qz-Or-Ab-An-H_2O. Contrib. Mineral. Petrol. 86, 264–273.
Johnson, M.C., Plank, T., 1999. Dehydration and melting experiments constrain the fate of subducted sediments. Geochemistry, Geophysics, Geosystems, p. 1.
Kagami, H., Yokose, H., Honma, H., 1989. ^{87}Sr/^{86}Sr and ^{143}Nd/^{144}Nd ratios of GSJ rock reference samples; JB-1a, JA-1 and JG-1a. Geochem. J. 23, 209–214.
Kelemen, P. B., Yogodzinski, G. M. Scholl, D. W., 2003. Along-strike variation in the Aleutian island arc: Genesis of high Mg# andesite and implications for continental crust. In *Inside the Subduction Factory* (ed Eiler, J.), Geophysical Monograph 138, American Geophysical Union, pp. 223-276.
Kelley, K.A., Plank, T., Farr, L., Ludden, J., Staudigel, H., 2005. Subduction cycling of U, Th, and Pb. Earth Planet. Sci. Lett. 234, 369–383.
Kerrick, D.M., Connolly, J.A.D., 2001. Metamorphic devolatilization of subducted marine sediments and the transport of volatiles into the Earth's mantle. Nature 411, 293–296.
Kessel, R., Schmidt, M.W., Ulmer, P., Pettke, T., 2005. Trace element signature of subduction-zone fluids, melts and supercritical liquids at 120–180 km depth. Nature 437, 724–727.
Kimura, J.-I., Nakajima, J., 2014. Behaviour of subducted water and its role in magma genesis in the NE Japan arc: A combined geophysical and geochemical approach. Geochim. Cosmochim. Acta 143, 165–188.
Kimura, J.-I., Kent, A.J.R., Rowe, M.C., Katakuse, M., Nakano, F., Hacker, B.R., van Keken, P.E., Kawabata, H., Stern, R.J., 2010. Origin of cross-chain geochemical variation in Quaternary lavas from the northern Izu arc: Using a quantitative mass balance approach to identify mantle sources and mantle wedge processes. Geochem. Geophys. Geosyst. 11, Q10011.
Kimura, J.-I., Gill, J.B., Kunikiyo, T., Osaka, I., Shimoshioiri, Y., Katakuse, M., Kakubuchi, S., Nagao, T., Furuyama, K., Kamei, A., Kawabata, H., Nakajima, J., van Keken, P.E., Stern, R.J., 2014. Diverse magmatic effects of subducting a hot slab in SW Japan: Results from forward modeling. Geochem. Geophys. Geosyst. 15, 691–739.
Kitamura, K., Ishikawa, M., Arima, M., 2003. Petrological model of the northern Izu–Bonin–Mariana arc crust: constraints from high-pressure measurements of elastic wave velocities of the Tanzawa plutonic rocks, central Japan. Tectonophysics 371, 213–221.
Kobayashi, K., Kasuga, S., Okino, K., 1995. Shikoku basin and its margins. In: Taylor, B. (Ed.), *Backarc Basins*. Springer, Boston, MA, pp. 381–405.
Konrad-Schmolke, M., Halama, R., Manea, V.C., 2016. Slab mantle dehydrates beneath Kamchatka—Yet recycles water into the deep mantle. Geochem. Geophys. Geosyst. 17, 2987–3007.
Kutsukake, T., 2002. Geochemical characteristics and variations of the Ryoke granitoids, southwest Japan: Petrogenetic implications for the plutonic rocks of a magmatic arc. Gond. Res. 5, 355–372.
Lee, C., Kim, Y., 2021. Role of warm subduction in the seismological properties of the forearc mantle: An example from Southwest Japan. Sci. Adv. 7, eabf8934.
Li, Y.-H., Ishihara, S., 2013. Compositional variation of the late Cretaceous–Paleogene plutons from southwest Japan and its implication for ore genesis and continental growth. J. Asian Earth Sci. 70–71, 142–159.
Li, X., Li, S., Zhang, Z., Zhong, Y., Li, D., 2024. Magnesium isotopic fractionation during post-serpentinization alteration: Implications for arc and oceanic Mg cycles. Chem. Geol. 648, 121866.
Li, W., Teng, F., Xiao, Y., 2018. Magnesium isotope record of fluid metasomatism along the slab-mantle interface in subduction zones. Geochim. Cosmochim. Acta 237, 312–319.
Li, S., Yang, W., Ke, S., Meng, X., Tian, H., Xu, L., He, Y., Huang, J., Wang, X., Xia, Q., Sun, W., Yang, X., Ren, Z., Wei, H., Liu, Y., Meng, F., Yan, J., 2017. Deep carbon cycles constrained by a large-scale mantle Mg isotope anomaly in eastern China. Natl. Sci. Rev. 4, 111–120.
Liu, X.N., Hin, R.C., Coath, C.D., van Soest, M., Melekhova, E., Elliott, T., 2022. Equilibrium olivine-melt Mg isotopic fractionation explains high δ^{26}Mg values in arc lavas. Geochem. Perspect. Lett. 22, 42–47.
Liu, X., Hin, R.C., Coath, C.D., Bizimis, M., Su, L., Ionov, D.A., Takazawa, E., Brooker, R., Elliott, T., 2023. The magnesium isotopic composition of the mantle. Geochim. Cosmochim. Acta 358, 12–26.
Liu, X.-F., Liu, X.-M., Zhai, S., Zhang, Z., Bi, D., Wang, X.-K., Cao, C., Liu, X., 2024. A dolomite-based record of seawater calcium isotope composition over the Neogene. Geochim. Cosmochim. Acta 368, 1–11.
Liu, S.-A., Teng, F.-Z., Yang, W., Wu, F.-Y., 2011. High-temperature inter-mineral magnesium isotope fractionation in mantle xenoliths from the North China craton. Earth Planet. Sci. Lett. 308, 131–140.
Liu, X.M., Teng, F.Z., Rudnick, R.L., McDonough, W.F., Cummings, M.L., 2014. Massive magnesium depletion and isotope fractionation in weathered basalts. Geochim. Cosmochim. Acta 135, 336–349.
Liu, P., Teng, F., Dick, H.J.B., Zhou, M., Chung, S., 2017. Magnesium isotopic composition of the oceanic mantle and oceanic Mg cycling. Geochim. Cosmochim. Acta 206, 151–165.
Lu, Y., Makishima, A., Nakamura, E., 2007. Coprecipitation of Ti, Mo, Sn and Sb with fluorides and application to determination of B, Ti, Zr, Nb, Mo, Sn, Sb, Hf and Ta by ICP-MS. Chem. Geol. 236, 13–26.
Makishima, A., Nakamura, E., 2006. Determination of major/minor and trace elements in silicate samples by ICP-QMS and ICP-SFMS applying isotope dilution-internal standardisation (ID-IS) and multi-stage internal standardisation. Geostand. Geoanal. Res. 30, 245–271.
Manning, C.E., 2004. The chemistry of subduction-zone fluids. Earth Planet. Sci. Lett. 223, 1–16.
Marschall, H. R., 2018. Boron isotopes in the ocean floor realm and the mantle. In Boron isotopes. Advances in Isotope Geochemistry (eds. H. Marschall and G. Foster). Springer, Cam. pp. 189-215.
Martin, C., Flores, K.E., Vitale-Brovarone, A., Angiboust, S., Harlow, G.E., 2020. Deep mantle serpentinization in subduction zones: Insight from in situ B isotopes in slab and mantle wedge serpentinites. Chem. Geol. 545, 119637.
McDonough, W.F., Rudnick, R.L., 1998. Mineralogy and composition of the upper mantle. Rev. Mineral. 37, 139–164.
McDonough, W.F., Sun, S.-S., 1995. The composition of the Earth. Chem. Geol. 120, 223–253.
Meng, Y., Yuan, H., Santosh, M., Mooney, W.D., Guo, L., 2021. Heavy magnesium isotopes in the Gangdese Magmatic Belt: Implications for magmatism in the Mesozoic subduction system of southern Tibet. Lithos 390–391, 106106.
Miyazaki, T., Shuto, K., 1998. Sr and Nd isotope ratios of twelve GSJ rock reference samples. Geochem. J. 32, 345–350.
Moriguti, T., Nakamura, E., 1998. Across-arc variation of Li isotopes in lavas and implications for crust/mantle recycling at subduction zones. Earth Planet. Sci. Lett. 163, 167–174.
Moriguti, T., Shibata, T., Nakamura, E., 2004. Lithium, boron and lead isotope and trace element systematics of Quaternary basaltic volcanic rocks in northeastern Japan: mineralogical controls on slab-derived fluid composition. Chem. Geol. 212, 81–100.
Nakajima, J., Tsuji, Y., Hasegawa, A., 2009. Seismic evidence for thermally-controlled dehydration reaction in subducting oceanic crust. Geophys. Res, Lett, p. 36.
Nakamura, E., Makishima, A., Moriguti, T., Kobayashi, K., Sakaguchi, C., Yokoyama, T., Tanaka, R., Kuritani, T., Takei, H., 2002. Comprehensive geochemical analyses of small amounts (< 100 mg) of extraterrestrial samples for the analytical competition related to the sample return mission MUSES-C. The Institute of Space and Astronautical Science Report. S.P.: The First Open Competition for the MUSES-C Asteroidal Sample Preliminary Examination Team, 16, 49-101.
Nesbitt, H., Young, G.M., 1982. Early Proterozoic climates and plate motions inferred from major element chemistry of lutites. Nature 299, 715–717.
Nguyen, T.T., Kitagawa, H., Pineda Velasco, I., Nakamura, E., 2020. Feedback of slab distortion on volcanic arc evolution: Geochemical perspective from late Cenozoic volcanism in SW Japan. Journal of Geophysical Research: Solid. Earth 125, e2019JB019143.
Ottolini, L., Le Fèvre, B., Vannucci, R., 2004. Direct assessment of mantle boron and lithium contents and distribution by SIMS analyses of peridotite minerals. Earth Planet. Sci. Lett. 228, 19–36.
Pagé, L., Hattori, K., 2019. Abyssal serpentinites: Transporting halogens from Earth's surface to the deep mantle. Minerals 9, 61.
Pan, D., Spanu, L., Harrison, B., Sverjensky, D.A., Galli, G., 2013. Dielectric properties of water under extreme conditions and transport of carbonates in the deep Earth. Proc. Natl. Acad. Sci. 110, 6646–6650.
Pang, K., Teng, F., Sun, Y., Chung, S., Zarrinkoub, M.H., 2020. Magnesium isotopic systematics of the Makran arc magmas, Iran: Implications for crust-mantle Mg isotopic balance. Geochim. Cosmochim. Acta 278, 110–121.
Peacock, S.M., 2001. Are the lower planes of double seismic zones caused by serpentine dehydration in subducting oceanic mantle? Geology 29, 299–302.

Peacock, S.M., Wang, K., 1999. Seismic consequences of warm versus cool subduction metamorphism: examples from Southwest and Northeast Japan. Science 286, 937–939.
Pearce, J.A., Peate, D.W., 1995. Tectonic implications of the composition of volcanic arc magmas. Annu. Rev. Earth Planet. Sci. 23, 251–285.
Pearce, C.R., Saldi, G.D., Schott, J., Oelkers, E.H., 2012. Isotopic fractionation during congruent dissolution, precipitation and at equilibrium: Evidence from Mg isotopes. Geochim. Cosmochim. Acta 92, 170–183.
Pineda-Velasco, I., Kitagawa, H., Nguyen, T.T., Kobayashi, K., Nakamura, E., 2018. Production of high-Sr andesite and dacite magmas by melting of subducting oceanic lithosphere at propagating slab tears. J. Geophys. Res. Solid Earth 123, 3698–3728.
Pirard, C., Hermann, J., 2015. Focused fluid transfer through the mantle above subduction zones. Geology 43, 915–918.
Plank, T., 2014. The Chemical Composition of Subducting Sediments. In: Holland, H.D., Turekian, K.K. (Eds.), *Treatise on Geochemistry*, Second Edition. Elsevier, Oxford, pp. 607–629.
Plank, T., Langmuir, C.H., 1998. The chemical composition of subducting sediment and its consequences for the crust and mantle. Chem. Geol. 145, 325–394.
Pogge Von Strandmann, P.A., Dohmen, R., Marschall, H.R., Schumacher, J.C., Elliott, T., 2015. Extreme magnesium isotope fractionation at outcrop scale records the mechanism and rate at which reaction fronts advance. J. Petrol. 56, 33–58.
Pogge Von Strandmann, P.A.E., Elliott, T., Marschall, H.R., Coath, C., Lai, Y., Jeffcoate, A.B., Ionov, D.A., 2011. Variations of Li and Mg isotope ratios in bulk chondrites and mantle xenoliths. Geochim. Cosmochim. Acta 75, 5247–5268.
Prigent, C., Warren, J.M., Kohli, A.H., Teyssier, C., 2020. Fracture-mediated deep seawater flow and mantle hydration on oceanic transform faults. Earth Planet. Sci. Lett. 532, 115988.
Ribeiro, J.M., Lee, C.A., 2017. An imbalance in the deep water cycle at subduction zones: The potential importance of the fore-arc mantle. Earth Planet. Sci. Lett. 479, 298–309.
Rojas-Kolomiets, E., Jensen, O., Bizimis, M., Yogodzinski, G., Ackerman, L., 2023. Serpentinite fluids and slab-melting in the Aleutian arc: Evidence from molybdenum isotopes and boron systematics. Earth Planet. Sci. Lett. 603, 117970.
Romer, R.L., Wawrzenitz, N., Oberhänsli, R., 2003. Anomalous unradiogenic $^{87}Sr/^{86}Sr$ ratios in ultrahigh-pressure crustal carbonates – evidence for fluid infiltration during deep subduction? Terra Nova 15, 330–336.
Sakuyama, M., Nesbitt, R.W., 1986. Geochemistry of the Quaternary volcanic rocks of the Northeast Japan arc. J. Vol. Geotherm. Res. 29, 413–450.
Savov, I.P., Ryan, J.G., D'Antonio, M., Kelley, K., Mattie, P., 2005. Geochemistry of serpentinized peridotites from the Mariana Forearc Conical Seamount, ODP Leg 125: Implications for the elemental recycling at subduction zones. Geochemistry, Geophysics, Geosystems, p. 6.
Savov, I.P., Ryan, J.G., D'Antonio, M., Fryer, P., 2007. Shallow slab fluid release across and along the Mariana arc-basin system: Insights from geochemistry of serpentinized peridotites from the Mariana fore arc. J. Geophys. Res. Solid Earth 112.
Scambelluri, M., Rampone, E., Piccardo, G.B., 2001. Fluid and element cycling in subducted serpentinite: a trace-element study of the Erro–Tobbio high-pressure ultramafites (Western Alps, NW Italy). J. Petrol. 42, 55–67.
Scambelluri, M., Pettke, T., Cannaò, E., 2015. Fluid-related inclusions in Alpine high-pressure peridotite reveal trace element recycling during subduction-zone dehydration of serpentinized mantle (Cima di Gagnone, Swiss Alps). Earth Planet. Sci. Lett. 429, 45–59.
Scambelluri, M., Cannaò, E., Gilio, M., 2019. The water and fluid-mobile element cycles during serpentinite subduction. A review. Eur. J. Mineral. 31, 405–428.
Schauble, E.A., 2011. First-principles estimates of equilibrium magnesium isotope fractionation in silicate, oxide, carbonate and hexaaquamagnesium(2+) crystals. Geochim. Cosmochim. Acta 75, 844–869.
Schmidt, M.W., Poli, S., 1998. Experimentally based water budgets for dehydrating slabs and consequences for arc magma generation. Earth Planet. Sci. Lett. 163, 361–379.
Sedaghatpour, F., Teng, F., Liu, Y., Sears, D.W.G., Taylor, L.A., 2013. Magnesium isotopic composition of the Moon. Geochim. Cosmochim. Acta 120, 1–16.
Shen, J., Li, S., Wang, S., Teng, F., Li, Q., Liu, Y., 2018. Subducted Mg-rich carbonates into the deep mantle wedge. Earth Planet. Sci. Lett. 503, 118–130.
Shibata, T., Nakamura, E., 1997. Across-arc variations of isotope and trace element compositions from Quaternary basaltic volcanic rocks in northeastern Japan: Implications for interaction between subducted oceanic slab and mantle wedge. Journal of Geophysical Research: Solid Earth 102, 8051–8064.
Shimoda, G., Tatsumi, Y., Nohda, S., Ishizaka, K., Jahn, B.M., 1998. Setouchi high-Mg andesites revisited: geochemical evidence for melting of subducting sediments. Earth Planet. Sci. Lett. 160, 479–492.
Spandler, C., Hermann, J., Faure, K., Mavrogenes, J.A., Arculus, R.J., 2008. The importance of talc and chlorite "hybrid" rocks for volatile recycling through subduction zones; evidence from the high-pressure subduction mélange of New Caledonia. Contrib. Mineral. Petrol. 155, 181–198.
Staudigel, H., Plank, T., White, B., Schmincke, H., 1996. Geochemical fluxes during seafloor alteration of the basaltic upper oceanic crust: DSDP Sites 417 and 418. In Subduction: Top to Bottom (eds G. E. Bebout, D. W. Scholl, S. H. Kirby and J. P. Platt). Geophys. Monogr. Ser. 96, 19–38.
Stracke, A., Tipper, E.T., Klemme, S., Bizimis, M., 2018. Mg isotope systematics during magmatic processes: Inter-mineral fractionation in mafic to ultramafic Hawaiian xenoliths. Geochim. Cosmochim. Acta 226, 192–205.
Su, B., Hu, Y., Teng, F., Qin, K., Bai, Y., Sakyi, P.A., Tang, D., 2017. Chromite-induced magnesium isotope fractionation during mafic magma differentiation. Sci. Bull. 62, 1538–1546.
Su, B., Hu, Y., Teng, F., Xiao, Y., Zhang, H., Sun, Y., Bai, Y., Zhu, B., Zhou, X., Ying, J., 2019. Light Mg isotopes in mantle-derived lavas caused by chromite crystallization, instead of carbonatite metasomatism. Earth Planet. Sci. Lett. 522, 79–86.
Sudo, M., Uto, K., Anno, K., Ishizuka, O., Uchiumi, S., 1998. SORI93 biotite: A new mineral standard for K-Ar dating. Geochem. J. 32, 49–58.
Sun, S.-S., McDonough, W.F., 1989. Chemical and isotopic systematics of oceanic basalts: implications for mantle composition and processes. Geol. Soc. Lond. Spec. Pub. 42, 313–345.
Suyehiro, K., Takahashi, N., Ariie, Y., Yokoi, Y., Hino, R., Shinohara, M., Kanazawa, T., Hirata, N., Tokuyama, H., Taira, A., 1996. Continental crust, crustal underplating, and low-Q upper mantle beneath an oceanic island arc. Science 272, 390–392.
Syracuse, E.M., van Keken, P.E., Abers, G.A., 2010. The global range of subduction zone thermal models. Phys. Earth Planet. Inter. 183, 73–90.
Taira, A., 1988. The Shimanto belt in Shikoku, Japan-evolution of Cretaceous to Miocene accretionary prism. Shimanto Belt, Modern Geology 12, 1–42.
Tan, D., Xiao, Y., Dai, L., Sun, H., Wang, Y., Gu, H., 2022. Differentiation between carbonate and silicate metasomatism based on lithium isotopic compositions of alkali basalts. Geology 50, 1150–1155.
Tani, K., Fiske, R.S., Dunkley, D.J., Ishizuka, O., Oikawa, T., Isobe, I., Tatsumi, Y., 2011. The Izu Peninsula, Japan: Zircon geochronology reveals a record of intra-oceanic rear-arc magmatism in an accreted block of Izu–Bonin upper crust. Earth Planet. Sci. Lett. 303, 225–239.
Tanimizu, M., Ishikawa, T., 2006. Development of rapid and precise Pb isotope analytical technique using MC-ICP-MS and new results for GSJ rock reference samples. Geochem. J. 40, 121–133.
Taylor, R.N., Nesbitt, R.W., 1998. Isotopic characteristics of subduction fluids in an intra-oceanic setting, Izu–Bonin Arc. Japan. Earth Planet. Sci. Lett. 164, 79–98.
Teng, F., 2017. Magnesium isotope geochemistry. Rev. Mineral. Geochem. 82, 219–287.
Teng, F.Z., Li, W.Y., Rudnick, R.L., Gardner, L.R., 2010b. Contrasting lithium and magnesium isotope fractionation during continental weathering. Earth Planet. Sci. Lett. 300, 63–71.
Teng, F.Z., Li, W.Y., Ke, S., Yang, W., Liu, S.A., Sedaghatpour, F., Wang, S.J., Huang, K.J., Hu, Y., Ling, M.X., 2015. Magnesium isotopic compositions of international geological reference materials. Geostand. Geoanal. Res. 39, 329–339.
Teng, F., Wadhwa, M., Helz, R.T., 2007. Investigation of magnesium isotope fractionation during basalt differentiation: Implications for a chondritic composition of the terrestrial mantle. Earth Planet. Sci. Lett. 261, 84–92.
Teng, F., Li, W., Ke, S., Marty, B., Dauphas, N., Huang, S., Wu, F., Pourmand, A., 2010a. Magnesium isotopic composition of the Earth and chondrites. Geochim. Cosmochim. Acta 74, 4150–4166.
Teng, F., Hu, Y., Chauvel, C., 2016. Magnesium isotope geochemistry in arc volcanism. Proc. Natl. Acad. Sci. 113, 7082–7087.
Tian, H., Yang, W., Li, S., Ke, S., Chu, Z., 2016. Origin of low $\delta^{26}Mg$ basalts with EM-I component: Evidence for interaction between enriched lithosphere and carbonated asthenosphere. Geochim. Cosmochim. Acta 188, 93–105.
Tian, H., Yang, W., Li, S., Ke, S., Duan, X., 2018. Low $\delta^{26}Mg$ volcanic rocks of Tengchong in Southwestern China: A deep carbon cycle induced by supercritical liquids. Geochim. Cosmochim. Acta 240, 191–219.
Tipper, E.T., Gaillardet, J., Louvat, P., Capmas, F., White, A.F., 2010. Mg isotope constraints on soil pore-fluid chemistry: Evidence from Santa Cruz. California. Geochim. Cosmochim. Acta 74, 3883–3896.
Togashi, S., Imai, N., Okuyama Kusunose, Y., Tanaka, T., Okai, T., Koma, T., Murata, Y., 2000. Young upper crustal chemical composition of the orogenic Japan Arc. Geochem. Geophys. Geosyst. 1, 1049.
Tonarini, S., Agostini, S., Doglioni, C., Innocenti, F., Manetti, P., 2007. Evidence for serpentinite fluid in convergent margin systems: The example of El Salvador (Central America) arc lavas. Geochem. Geophys. Geosyst. 8, Q09014.
Tonarini, S., Leeman, W.P., Leat, P.T., 2011. Subduction erosion of forearc mantle wedge implicated in the genesis of the South Sandwich Island (SSI) arc: Evidence from boron isotope systematics. Earth Planet. Sci. Lett. 301, 275–284.
Ulmer, P., Trommsdorff, V., 1995. Serpentine stability to mantle depths and subduction-related magmatism. Science 268, 858–861.
Utsu, T., 1974. Space-time pattern of large earthquakes occurring off the Pacific coast of the Japanese islands. J. Phys. Earth 22, 325–342.
van Keken, P.E., Wilson, C.R., 2023. An introductory review of the thermal structure of subduction zones: III—Comparison between models and observations. Prog Earth Planet Sci 10, 57.
Veizer, J., 1983. Trace elements and isotopes in sedimentary carbonates. In: Ribbe, P.H. (Ed.), *Carbonates: Mineralogy and Chemistry*, Review in Mineralogy, vol. 11. Mineralogical Society of America, Washington, D. C.
Wada, I., Wang, K., 2009. Common depth of slab-mantle decoupling: Reconciling diversity and uniformity of subduction zones. Geochem. Geophys. Geosyst. 10, Q10009.
Walowski, K.J., Wallace, P.J., Hauri, E.H., Wada, I., Clynne, M.A., 2015. Slab melting beneath the Cascade Arc driven by dehydration of altered oceanic peridotite. Nat. Geosci. 8, 404–408.
Wang, X., Chen, L., Hanyu, T., Zhong, Y., Shi, J., Liu, X., Kawabata, H., Zeng, G., Xie, L., 2021. Magnesium isotopic fractionation during basalt differentiation as recorded by evolved magmas. Earth Planet. Sci. Lett. 565, 116954.
Wang, Y., He, Y., Ke, S., 2020. Mg isotope fractionation during partial melting of garnet-bearing sources: An adakite perspective. Chem. Geol. 537, 119478.
Wang, Y., Deng, J., Liao, R., Chen, L., Li, D., Liu, H., Sun, W., 2023. Magnesium isotopic composition of the Mariana forearc serpentinite: Implications for Mg isotopic composition of the mantle wedge and Mg isotopic fractionation during mantle wedge serpentinization. Chem. Geol. 624, 121428.

Wang, Z., Liu, S., Ke, S., Liu, Y., Li, S., 2016. Magnesium isotopic heterogeneity across the cratonic lithosphere in eastern China and its origins. Earth Planet. Sci. Lett. 451, 77–88.
Wang, S.-J., Teng, F.-Z., Li, S.-G., 2014. Tracing carbonate-silicate interaction during subduction using magnesium and oxygen isotopes. Nat. Commun. 5, 5328.
Wang, S.J., Teng, F.Z., Bea, F., 2015. Magnesium isotopic systematics of metapelite in the deep crust and implications for granite petrogenesis. Geochem. Perspect. Lett. 1, 75–83.
Wang, S., Teng, F., Li, S., Zhang, L., Du, J., He, Y., Niu, Y., 2017. Tracing subduction zone fluid-rock interactions using trace element and Mg-Sr-Nd isotopes. Lithos 290–291, 94–103.
Wawrzenitz, N., Romer, R.L., Grasemann, B., Morales, L.G., 2019. Pre-UHP titanite archives pro- and retrograde episodes of fluid-marble-interaction (Dabie Shan UHP unit, China). Lithos 350–351, 105232.
Wendlandt, R.F., Mysen, B.O., 1980. Melting phase relations of natural peridotite + CO_2 as a function of degree of partial melting at 15 and 30 kbar. Am. Miner. 65, 37–44.
Workman, R.K., Hart, S.R., 2005. Major and trace element composition of the depleted MORB mantle (DMM). Earth Planet. Sci. Lett. 231, 53–72.
Xiong, J., Chen, Y., Ma, H., Schertl, H., Zheng, Y., Zhao, K., 2022. Tourmaline boron isotopes trace metasomatism by serpentinite-derived fluid in continental subduction zone. Geochim. Cosmochim. Acta 320, 122–142.
Yamamoto, M., Kagami, H., Narita, A., Maruyama, T., Kondo, A., Abe, S., Takeda, R., 2013. Sr and Nd isotopic compositions of mafic xenoliths and volcanic rocks from the Oga Peninsula, Northeast Japan Arc: Genetic relationship between lower crust and arc magmas. Lithos 162–163, 88–106.
Yang, W., Teng, F., Zhang, H., Li, S., 2012. Magnesium isotopic systematics of continental basalts from the North China craton: Implications for tracing subducted carbonate in the mantle. Chem. Geol. 328, 185–194.
Yang, W., Teng, F., Li, W., Liu, S., Shan, K., Liu, Y., Zhang, H., Gao, S., 2016. Magnesium isotopic composition of the deep continental crust. Am. Miner. 101, 243–252.
Yaxley, G.M., Green, D.H., 1994. Experimental demonstration of refractory carbonate-bearing eclogite and siliceous melt in the subduction regime. Earth Planet. Sci. Lett. 128, 313–325.
Yokoyama, T., Makishima, A., Nakamura, E., 1999. Evaluation of the coprecipitation of incompatible trace elements with fluoride during silicate rock dissolution by acid digestion. Chem. Geol. 157, 175–187.
Yokoyama, T., Kobayashi, K., Kuritani, T., Nakamura, E., 2003. Mantle metasomatism and rapid ascent of slab components beneath island arcs: Evidence from ^{238}U-^{230}Th-^{226}Ra disequilibria of Miyakejima volcano, Izu arc, Japan. J. Geophys. Res. Solid Earth 108, 2329.
Young, E.D., Tonui, E., Manning, C.E., Schauble, E., Macris, C.A., 2009. Spinel–olivine magnesium isotope thermometry in the mantle and implications for the Mg isotopic composition of Earth. Earth Planet. Sci. Lett. 288, 524–533.
Yuan, S., Li, H., Arculus, R.J., He, Y., Ke, S., Sun, W., 2023. Heavy magnesium isotopic compositions of basalts erupted during arc inception: Implications for the mantle source underlying the nascent Izu-Bonin-Mariana arc. Geochim. Cosmochim. Acta 352, 14–23.
Zellmer, G.F., 2008. Some first-order observations on magma transfer from mantle wedge to upper crust at volcanic arcs. Geol. Soc. Lond. Spec. Publ. 304, 15–31.
Zhang, W., Tanaka, R., Kitagawa, H., Bohlin, M., Nakamura, E., 2022. A rapid method of simultaneous chromatographic purification of Li and Mg for isotopic analyses using MC-ICP-MS. Int. J. Mass Spectrom. 480, 116893.
Zhang, W., Kitagawa, H., Nakamura, E., 2023. Lithium isotope constraints on slab and mantle contribution to arc magmas. Journal of Geophysical Research: Solid Earth, e2022JB025670.
Zhao, M., Chen, Y., Xiong, J., Zheng, Y., Zha, X., Huang, F., 2023. Element mobility and Mg isotope fractionation during peridotite serpentinization. Geochim. Cosmochim. Acta 340, 21–37.
Zhao, D., Yanada, T., Hasegawa, A., Umino, N., Wei, W., 2012. Imaging the subducting slabs and mantle upwelling under the Japan Islands. Geophys. J. Int. 190, 816–828.
Zhong, Y., Chen, L., Wang, X., Zhang, G., Xie, L., Zeng, G., 2017. Magnesium isotopic variation of oceanic island basalts generated by partial melting and crustal recycling. Earth Planet. Sci. Lett. 463, 127–135.